## scientific reports



### **OPEN**

# HIL co-simulation of an optimal hybrid fractional-order type-2 fuzzy PID regulator based on dSPACE for quadruple tank system

Faycal Medjili<sup>1</sup>, Abderrahmen Bouguerra<sup>2</sup>, Mohamed Ladjal<sup>1,3</sup>, Badreddine Babes<sup>4</sup>, Enas Ali<sup>5</sup>, Sherif S. M. Ghoneim<sup>6</sup>, Dessalegn Bitew Aeggegn<sup>7⊠</sup> & Ahmed B. Abou Sharaf<sup>8,9</sup>

Accurate regulation of the liquid level in a quadruple tank system (QTS) is not easy and imposes higher requirements on control strategies, so the design of controllers in these systems is challenging due to the difficulty of dynamic analysis of its nonlinear characteristics and parametric uncertainties. To overcome these problems in liquid level regulation and increase the robustness to the pump coefficients, this article proposes and investigates the use of an optimal hybrid fractional-order type-2 fuzzy-PID (OH-FO-T2F-PID) regulator using a combination of two bio-inspired evolutionary optimizers, namely augmented grey wolf optimizer and cuckoo search optimizer, which gives rise to the new hybrid A-GWOCS algorithm. This control mechanism was chosen to facilitate the convergence of the water liquids in the two tanks as quickly as possible to the corresponding required values. In addition, a collaborative optimization technique with several objectives is used to adjust the regulator parameters. The capability and efficiency of the suggested regulator is first investigated through computer simulation results and then confirmed by real-time control experimental results on the QTS based on dSPACE 1104 computation engine. The findings showed that the suggested OH-FO-T2F-PID regulator significantly outperformed both the optimized ADRC and the OH-FO-T1F-PID regulators. Specifically, it reduced the rising time by 17.02% and 95.21%, respectively, and the settling time by 25.13% and 74.28%. Additionally, the designed OH-FO-T2F-PID regulator successfully eliminated the steady-state error and overshoot, enabling precise regulation of the QTS, and maintenance the liquid level at the desired set point under a wide range of working situations. The robustness of the recommended regulator is also studied by considering - 50% disturbance in the QTS parameters, and the findings showed that the OH-FO-T2F-PID regulator is less susceptible to variations in parameters.

**Keywords** Quadruple tank system (QTS), Optimal hybrid fractional order type 2 fuzzy PID regulator, Hybrid A-GWOCSO algorithm, Multi-objective optimization, dSPACE 1104 computation engine

#### List of symbols

 $egin{array}{ll} A_i & {
m Cross-sectional \ areas \ of \ the \ tanks} \ h_1, h_2 & {
m Water \ level \ in \ tanks} \ 1 \ {
m and} \ 2} \ {
m Cross-sectional \ areas \ of \ the \ outlets} \ {
m g} & {
m Acceleration \ of \ gravity} \ \end{array}$ 

 $\eta_c$  Constant relating the control input with water inflow from the pumps

<sup>1</sup>Department of Electronics, Faculty of Technology, University of M'sila, University Pole, Bordj Bou Arreridj Road, 28000 M'sila, Algeria. <sup>2</sup>LGE Research Laboratory, Department of Electrical Engineering, Faculty of Technology, University of M'sila, University Pole, Bordj Bou Arreridj Road, 28000 M'sila, Algeria. <sup>3</sup>LASS, Laboratory of Analysis of Signals and Systems, Department of Electronics, Faculty of Technology, University of M'sila, University Pole, Bordj Bou Arreridj Road, 28000 M'sila, Algeria. <sup>4</sup>Research Center in Industrial Technologies CRTI, Algiers, Algeria. <sup>5</sup>University Centre for Research and Development, Chandigarh University, Mohali, Punjab 140413, India. <sup>6</sup>Department of Electrical Engineering, College of Engineering, Taif University, 21944 Taif, Saudi Arabia. <sup>7</sup>Department of Electrical and Computer Engineering, Debre Markos University, 269 Debre Markos, Ethiopia. <sup>8</sup>Ministry of Higher Education and Scientific Research, Industrial Technical Institute in Mataria, Cairo 11718, Egypt. <sup>9</sup>Centre for Research Impact and Outcome, Chitkara University Institute of Engineering and Technology, Chitkara University, Rajpura, Punjab 140401, India. <sup>∞</sup>email: dessalegn\_bitew@dmu.edu.et

 $v_1$ ,  $v_2$  Voltages supplied to pumps 1 and 2

 $\vec{k_1}, \vec{k_2}$  Coefficient of pump

**Greek symbols** 

 $y_1$  Divides flow from pump 1 to tanks 1 and 4 Divides flow from pump 2 to the tanks 2 and 3

 $\sigma_1, \sigma_2$  Disturbances

Abbreviations

QTS Quadruple tank system

OH-FO-T2F-PID Optimal hybrid fractional-order type-2 fuzzy-PID

A-GWO Augmented grey wolf optimizer
CSO Cuckoo search optimizer

A-GWOCSO Augmented grey wolf optimizer cuckoo search optimizer

MIMO Multiple inputs, multiple outputs **SISO** Single input, single output PID Proportional integral differential T1-FLS Type-1 fuzzy logic system Membership functions MFs ΑI Artificial intelligence **PSS** Power system stabilizer **FOCs** Fractional order calculus

FO-T2F-PID Fractional-order type-2 fuzzy-PID

FO Fraction-order AS Active suspension **PSU** Pumped storage unit TSK Takagi-Sugeno-Kang **GWO** Grey wolf optimizer **PSO** Particle swarm optimizer Cuckoo search optimizer CS **ACO** Ant colony optimizer Bacterial foraging optimizer **BFO** 

hyHS-RSA Hybridized harmony search-random search algorithm

CSA Crow-search algorithm SWA Spider wasp algorithm

RW-ARA Random walk aided artificial rabbits algorithm

HIL Hardware-in-the-loop FOU Footprint of uncertainty STD Standard deviations

ADRC Active disturbance rejection control

hAGWOCS Hybrid augmented grey wolf optimizer cuckoo search optimizer

GSO Gravitational search optimizer
DEO Differential evolution optimizer

FFO Fruit fly optimizer
ALA Ant lion algorithm

SOSO Symbiotic organisms search optimizer

BO Bat optimizer

FPO Flower pollination optimizer

FO Firefly optimizer
GO Genetic optimizer

GOA Grasshopper optimization algorithm

MFO Moth-flame algorithm
MVA Multiverse algorithm
DO Dragonfly optimizer
BBO Binary bat optimizer
BA Biogeography algorithm

BGSO Binary gravitational search optimizer

SCO Sine cosine optimizer
SSO Salp swarm optimizer
WOA Whale optimization algorithm
BMFA1, BMFA2 Binary moth flame algorithm
E-GWO Enhanced grey wolf optimizer

Liquid level control is extensively utilized in modern manufacturing processes, such as pharmaceutical system and petrochemical processing plant, wastewater treatment system, filtration, food processing, nuclear power production, and many others. Controlling the liquid level with the least amount of error or tracking the desired level in a QTS is a very difficult problem due to the nonlinear dynamics behavior and the uncertainties presented by the environment<sup>1</sup>. QTS is a particular group of unstable non-minimum phase MIMO (multiple inputs, multiple outputs) system. In practice, the implementation of regulators for a non-linear MIMO systems is far more complicated than for a SISO (single input, single output) systems, due to variations in process dynamics that typically result from the changing of operating points, as well as from interacting loops based on gate valve

ratio, in which each controlled variable affects more than one or all of the controlled variables. Moreover, QTS is susceptible to physical changes due to gradual deterioration or deformation of some components. A perfect liquid level regulation plays a very significant role in these nonlinear systems in view of the economic operation. For this reason, quite a few researchers have worked on it<sup>2</sup>. To reach the desired operating points as quickly as possible and maintain a stable level condition in tanks, numerous regulators have been developed for liquid level regulation of QTS. Among them we note, for example proportional integral differential (PID) regulator<sup>3</sup>, adaptive regulator<sup>4</sup>, backstepping regulator<sup>5</sup>, sliding mode regulator<sup>6</sup>, active disturbance rejection regulator<sup>7</sup>, fuzzy regulator<sup>8</sup>, predictive regulator<sup>9</sup>, linearized feedback regulator<sup>10</sup> and fractional order regulator<sup>11</sup>.

Some of these regulators, such as predictive and backstepping regulators are a model-based design approach and necessitate prior knowledge of QTS. On the other hand, a complete QTS system usually comprises of valves, sensors, conduits, pumps, reservoirs, and a few electrical and mechanical parts. During operation, and depending on the requirements, the valves can modify the opening, or the type of liquid in the reservoir can vary. Furthermore, some parameters may still be unknown in certain cases, for example the dimension, the discharge ratio of the valves, and the source voltage of the pump. As a result, developing a precise mathematical model for QTS is difficult. However, the Fuzzy regulators developed using a mathematical modelling approach are model-independent regulators<sup>12</sup>, allowing the QTS to be controlled without the need of decoupling, having as a logical basis the behaviour of the QTS at each of its stages. This makes the Fuzzy regulator a useful regulator for QTS. Most of the Fuzzy regulator applications have taken into account a Type-1 Fuzzy Logic System (T1-FLS). Nevertheless, T1-FLS is sometimes not satisfactory to overcome uncertainties because its membership functions (MFs) are completely crisp. Further, in 1975, a new breakthrough structure, known as Type-2 Fuzzy Sets, was originally designed to the regulator field by Zadeh<sup>13</sup> as a branch of Artificial Intelligence (AI) tools to deal with uncertainty in inputs, outputs, and decisions due to their many adjustable parameters, that make them useful for control applications, where the MFs have a fuzzy interval shape<sup>14</sup>, which is discussed in Cao et al.<sup>15</sup>.

The Type-2 Fuzzy regulator offers enhanced performance compared to the Type-1 Fuzzy regulator and has been utilized in different engineering fields such as automatic redundant control<sup>16</sup>, power system stabilizer (PSS) control<sup>17</sup>, aircraft flight control<sup>18</sup>, permanent magnet synchronous motor control<sup>19</sup>, automatic generation control of diverse energy source-based multiarea power system<sup>20</sup>, etc. Moreover, integrating the Type-2 Fuzzy regulator with Fractional Order Calculus (FOCs) can improve its efficiency<sup>21</sup>.

Over the past 20 years, FOCs has become more and more important in the design of advanced and resilient FO-T2F-PID regulators. This has increased the system's performance and robustness in the face of plant uncertainties due to the adoption of fraction-orders (FOs) of integrals and derivatives<sup>22,23</sup>. Applications for FO-T2F-PID regulators are many and include structural seismic control<sup>24</sup>, active suspension (AS) control<sup>25</sup>, pumped storage unit (PSU) control<sup>26</sup>, and wind turbine control<sup>27</sup>. The literature shows that adding FOCs to a Type 2 Fuzzy regulator can increase the stability of the feedback control system. Thus, combining FO terms with a Type 2 Fuzzy regulator will expand the search possibilities and increase the flexibility of the regulator. This feature motivated to design FO-T2F-PID regulator for the system under study which is highly uncertain and non-linear system. The primary contribution of this article is that it is the first to suggest an examination of the FO-T2F-PID regulator for QTS control, which lowers the control effort and improves the accuracy of monitored water levels. In order to apply the FO-T2F-PID regulator to QTS and exploit its distinct advantages in these systems, the Takagi–Sugeno–Kang (TSK) method is utilized. Fine-tuning of the FO terms and regulator parameters are the basic requirements for an effective control strategy. Therefore, the development of optimization tools can simplify the tuning of these parameters <sup>28</sup>.

In the last few decades, some scientists and academics have suggested a variety of evolutionary and heuristic optimization methods in order to address the optimization issues of benchmark and practical applications<sup>29</sup>. Here are the most popular among them: the grey wolf optimizer (GWO)<sup>30</sup>, particle swarm optimizer (PSO)<sup>31</sup>, cuckoo search optimizer (CSO)<sup>32</sup>, ant colony optimizer (ACO)<sup>33</sup>, bacterial foraging optimizer (BFO)<sup>34</sup>, hybridized harmony search-random search algorithm (hyHS-RSA)<sup>35</sup>, crow-search algorithm (CSA)<sup>36</sup>, pelican algorithm (PA)<sup>37</sup>, golden eagle algorithm (GEA)<sup>38</sup>, improved cooperation search algorithm (I-CSA)<sup>39</sup>, spider wasp algorithm (SWA)<sup>40</sup>, and random walk aided artificial rabbits algorithm (RW-ARA)<sup>41</sup>.

GWO is a meta-heuristic intelligent optimization method inspired by the social structure and hunting tactics of grey wolves in the wild. The benefits of this optimizer include increased flexibility, reduced optimization settings, strong adaptability, and simplicity of implementation. Recently, an improved version of GWO has been developed with more exploration capabilities, called Augmented-GWO (A-GWO). However, in some cases, the performance of A-GWO is very poor at the exploitation stage and remains stagnant at the local optimum. Conversely, CS is a population-based search technique that draws inspiration from the distinctive nesting habits of Cuckoo birds. Multiple research studies have shown that the CS favours global exploration<sup>42</sup>. CSs have been extensively combined with other optimizers to increase their capacity to avoid local optima<sup>43</sup>. The selection of optimizer depends on the control objectives and the specific features of the system, and a mixture of diverse optimizers may be indispensable to attain the desired performance<sup>44</sup>.

In contrast to conventional optimization techniques, a new hybrid optimizer called Hybrid A-GWOCSO algorithm is developed in this article, which effectively achieves global optimization with minimal computation time by combining the best features of two bio-inspired evolutionary optimization (AGWO & CS). The new hybrid A-GWOCSO algorithm combines the exploitation capabilities of A-GWO with the exploration capabilities of CS. So, this research suggests a hybrid A-GWOCSO technique to select the best parameters in FO-T2F-PID regulator. As far as we know, there has been no effort to extract the gains of the FO-T2F-PID regulator by hybridizing A-GWO and CS. This effective tuning method along with the Type-2 Fuzzy embedded FO-PID regulator increases the effectiveness of the suggested control method in regulating the water level of QTS.

Hardware-in-the-loop (HIL) Co-Simulation is a type of real-time simulation in which a specific component of hardware interfaces interacts with a mathematical model or simulation environment. Using HIL application

reduces costs, testing times and dangerous scenarios, since it is built on an interactive simulation and it is piloted by a process or regulator operating on a digital platform that interacts with the regulator or real process<sup>31</sup>.

#### Research gap

Despite extensive research on the control of QTS, there are still many research gaps and open challenges. Here are some potential research gaps in the control of QTS:

- Most existing control strategies for QTS concentrate on linearized models or assume near-linear behavior. However, the QTS displays considerable nonlinearities, particularly at extreme operating points.
- Many of the above control strategies have only been validated in simulation, with limited consideration of real-time implementation constraints, such as computational delays, sampling rates, or hardware limitations.
- Existing control strategies often focus on a single objective (e.g., stability or set-point tracking), neglecting trade-offs between competing objectives (e.g., control inputs, robustness, and performance).
- Although the FO-T2F-PID regulator has been extensively employed in the control of various systems, experimental confirmation of its usage in QTS is still limited.
- Hybrid A-GWOCSO method is essential for the reliable control of QTS, but its integration with FO-T2F-PID regulator for QTS control is still largely unexplored.

#### Motivation and contribution

Being able to effectively control liquid levels in multiple tanks simultaneously is crucial for the efficiency and safety of QTS. If the levels aren't properly controlled, it can lead to overflow, undersupply, or other malfunctions. In addition, there might be constraints on the inputs, like the flow rates being limited, or delays in the system due to the time it takes for liquid to move from one tank to another. These factors can complicate the control strategy of QTS. To fulfill the above-mentioned goals, suitable control technique should be developed to deal with these challenges. Amongst the many regulators suggested in the literature, FO-T2F-PID regulator is the one that is most frequently utilized. Due to a variety of FO-T2F-PID regulator gains, the Hybrid A-GWOCSO method is employed to obtain the best results and the most effective solutions. Many researchers have suggested the Hybrid A-GWOCSO to optimize the regulator gains, though it takes more time and becomes stagnant while searching for the global optimum. The Hybrid A-GWOCSO is utilized in the study since the optimized FO-T2F-PID regulator has not been investigated extensively. The important contributions of this article are as follows:

- *Novel regulator design*: This research proposes a new control system that combines the advantages of Fuzzy Type 2 and FOCs in a single regulator called HO-FO-T2F-PID that effectively handles modelling and parameter uncertainty in QTS, providing a more robust and adaptable solution.
- Real-time implementation: This article uses HIL technology to simulate the application of an OH-FO-T2F-PID regulator on a QTS, which allows us to evaluate the effectiveness of the recommended controller in real-time application. Additionally, the performance of the recommended regulator will be compared with that of the OH-FO-T1F-PID and optimized ADRC regulators, and the Hybrid A-GWOCSO method was also used to adjust each regulator under study.
- Noise sensitivity reduction: The HO-FO-T2F-PID regulator can smooth out its response to sudden changes
  in the liquid level, thereby reducing the impact of high-frequency noise. This results in smoother QTS performance.
- Significance and advancement of the field: This study contributes significantly to the development of the field of QTS control, presenting a robust, flexible and high-performance control strategy that fills the gap between theory developments and real-world application.
- Advanced optimization using Hybrid A-GWOCSO method: Exploiting the newly developed meta-heuristic optimization algorithm (i.e. AGWO and CS) to precisely adjust the parameters of the suggested HO-FO-T2F-PID regulator. The capability of the hybrid A-GWOCSO to balance the exploration and exploitation stages leads to improved statistical outcomes compared to 23 other metaheuristic methods.
- Excellent performance: A fair performance comparison with the OH-FO-T1F-PID and optimized ADRC regulator has proven the superiority and competence of the proposed OH-FO-T2F-PID regulator in terms of response time, accuracy, and robustness, especially under different working situations and disturbances.

#### Work structure

The organization of the study is as follows: Section "Description and structural model of QTS" describes the QTS modelling procedure. Section "Regulator construction" gives a comprehensive overview of the suggested control strategy, which includes FOCs and Fuzzy Type 2. Section "Hybridized algorithm for regulator parameter tuning" discusses the proposed hybrid A-GWOCSO algorithm, which is used to adjust the coefficients of the considered regulator. Section "Statistical evaluation of the proposed hAGWOCS method" presents the quantitative and qualitative analysis, along with a statistical comparison of the proposed Hybrid A-GWOCSO with 23 recently reported optimizer. Sections "Simulation tests" and "HIL experiment validation" discuss and analyze the outcomes obtained from simulations and HIL Co-Simulation, respectively. Finally, Section "Conclusion and future scope" provides the general conclusion of the study and discusses the suggested method's contribution to improving the QTS control with the future works.

#### Description and structural model of QTS

The schematic of the structural model of the QTS under consideration is illustrated in Fig. 1. The system contains two variable speed pumps (called Pump 1 and Pump 2) driven by DC motors to move water from the liquid basin to four overhead tanks located in the same area. The tanks located above (designated as Tank 3 and Tank

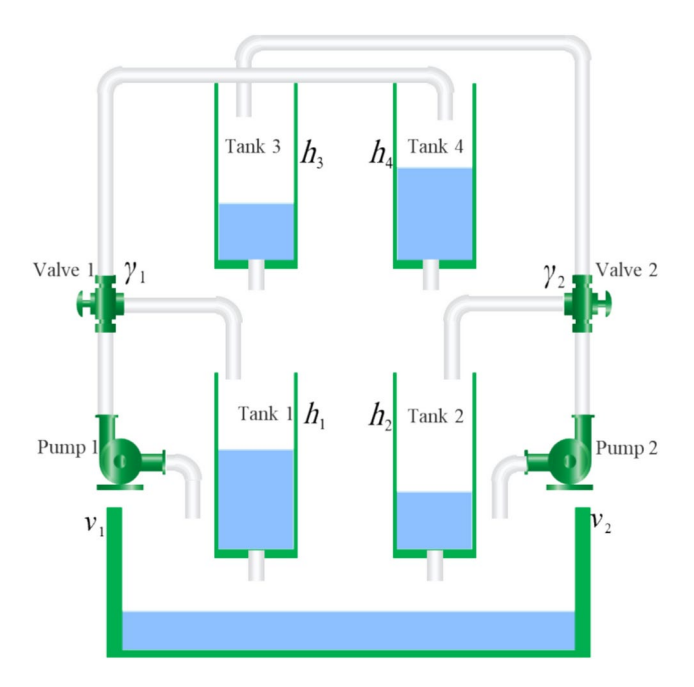


Fig. 1. A complete representation of QTS.

4) freely empty into the tanks located below (denoted as Tank 1 and Tank 2). Level sensors detect the water levels in these two lower tanks (designated as  $h_1$  and  $h_2$ ) and provide an output signal proportional to the liquid level. The motor terminal voltage ( $v_1$  and  $v_2$ ) determines the flow rate delivered by each pump.

The goal is to adjust the voltages supplied to pumps 1 and 2 (represented by  $v_1$  and  $v_2$ ) so that the liquid levels in the two inferior tanks converge to their corresponding reference levels (represented by  $h_{d1}$  and  $h_{d2}$ ). This article does not address the control of liquid levels in the overhead tanks marked as  $h_3$  and  $h_4$ . The differential equations below describe the dynamic equations of QTS with respect to mass balance and Bernoulli's laws:

$$\begin{cases} \frac{dh_1}{dt} = -\frac{a_1}{A_1}\sqrt{2gh_1} + \frac{a_3}{A_1}\sqrt{2gh_3} + \frac{\gamma_1 k_1}{A_1}v_1 + \sigma_1\\ \frac{dh_2}{dt} = -\frac{a_2}{A_2}\sqrt{2gh_2} + \frac{a_4}{A_2}\sqrt{2gh_4} + \frac{\gamma_2 k_2}{A_2}v_2 + \sigma_2\\ \frac{dh_3}{dt} = -\frac{a_3}{A_3}\sqrt{2gh_3} + \frac{(1-\gamma_1)k_2}{A_3}v_2\\ \frac{dh_4}{dt} = -\frac{a_4}{A_4}\sqrt{2gh_4} + \frac{(1-\gamma_1)k_1}{A_4}v_1 \end{cases}$$
(1)

The area of the tank flow opening can be indicated by the coefficient  $a_p$  where  $i=1,\ldots,4$ . The area of tank i can be indicated by the coefficient  $A_p$  where  $i=1,\ldots,4$ . The coefficient of pump can be represented by the variable  $k_p$  where j=1,2 (i.e., the water flow rate produced by pump j). The external disturbances caused by flow rate can be represented by  $\sigma_1$  and  $\sigma_2$ .

Some other variables of the QTS can also be mentioned, such as the inflow to tank 1  $(\gamma_1 k_1 \nu_1)$ , the inflow to tank 4  $(1 - \gamma_1)$ .  $k_1 \nu_1$ , the inflow to tank 2  $(\gamma_2 k_2 \nu_2)$  and finally the inflow to tank 3  $(1 - \gamma_2)$ .  $k_2 \nu_2$ . The symbol g stands for the gravitational acceleration.

The QTS is a minimum-phase system if the total water flow rates of the higher tanks are less than the comparable total of the lower tanks<sup>10</sup>  $(1 < \gamma_1 + \gamma_2 < 2)$ . Otherwise  $(0 < \gamma_1 + \gamma_2 < 1)$ , the QTS is a non-minimum phase system. The state, input and output vectors of QTS are defined by x, u, and y, respectively.

$$x = [h_1 h_2 h_3 h_4]^T$$
,  $u = [v_1 v_2]^T$ , and  $y = [h_1 h_2]^T$ .

Therefore, the state-space equation for QTS becomes as follows:

$$\begin{bmatrix} \dot{x}_1 \\ \dot{x}_2 \\ \dot{x}_3 \\ \dot{x}_4 \end{bmatrix} = \begin{bmatrix} -\frac{a_1}{A_1} \sqrt{2gh_1} + \frac{a_3}{A_1} \sqrt{2gh_3} \\ -\frac{a_2}{A_2} \sqrt{2gh_2} + \frac{a_4}{A_2} \sqrt{2gh_4} \\ -\frac{a_3}{A_3} \sqrt{2gh_3} \\ -\frac{a_4}{A_4} \sqrt{2gh_4} \end{bmatrix} + \begin{bmatrix} \frac{(1-\gamma_1)k_1}{A_4} & 0 \\ 0 & \frac{\gamma_2 k_2}{A_2} \\ 0 & \frac{(1-\gamma_1)k_2}{A_3} \\ \frac{(1-\gamma_1)k_1}{A_4} & 0 \end{bmatrix} \begin{bmatrix} v_1 \\ v_2 \end{bmatrix} + \begin{bmatrix} \sigma_1 \\ \sigma_2 \end{bmatrix}$$
(2)

Using the formula for measurement:

$$\begin{bmatrix} y_1 \\ y_2 \end{bmatrix} = \begin{bmatrix} n_c & 0 & 0 & 0 \\ 0 & n_c & 0 & 0 \end{bmatrix} \begin{bmatrix} h_1 \\ h_2 \\ h_3 \\ h_4 \end{bmatrix}$$
 (3)

Symbol	Value/unit
$a_{1}, a_{3}$	0.075 cm <sup>2</sup>
a <sub>2</sub> , a <sub>4</sub>	0.055 cm
$A_1, A_2, A_3, A_4$	35 cm <sup>2</sup>
$k_1$	3.51cm <sup>3</sup> /volt.s
$k_2$	3.58cm <sup>3</sup> /volt.s
$\gamma_1$	0.6
$\gamma_2$	0.7
g	9.81 m s <sup>-2</sup>
$n_c$	1 cm/s <sup>2</sup>

Table 1. Model specifications of the QTS.

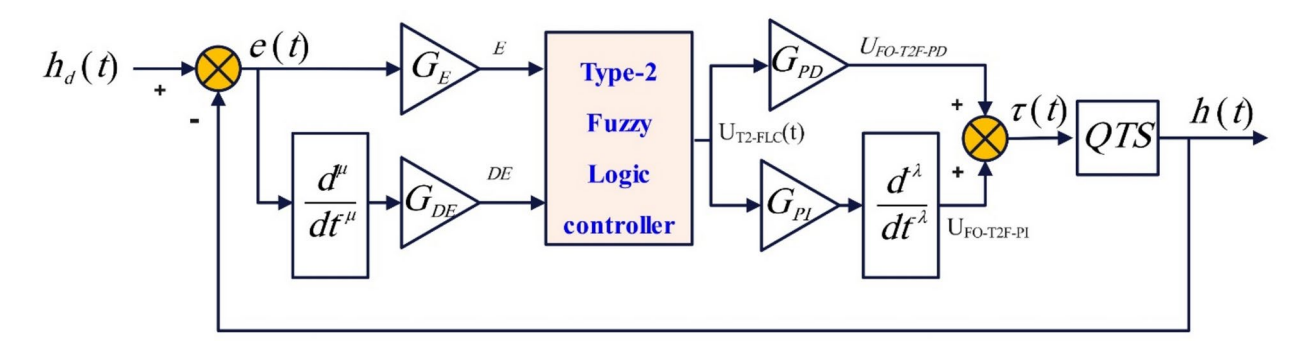


Fig. 2. Block scheme of the suggested OH-FO-T2F-PID regulator applied to QTS.

where  $n_c$  is the calibrated constant. It is also possible to express the QTS state space model in the form of vector fields as:

$$\dot{x} = F(x) + G(x)v + \sigma \tag{4}$$

where  $\dot{x} \in R^{4\times 1}$ ,  $F \in R^{4\times 1}$ ,  $G \in R^{2\times 1}$ ,  $v \in R^{2\times 1}$ , and  $\sigma \in R^{2\times 1}$ .

Table 1 provides a description of the operational variables of the QTS.

#### Regulator construction

The main goal of this research study is to develop and construct an effective regulator that allows the QTS to quickly reach a new equilibrium point in the in the existence of external perturbations, while the fluid levels in the two lower tanks follow the desired set point values, i.e.,  $h_1$  and  $h_2$ . For this reason, the structural design and planning procedures of the OH-FO-T2F-PID regulator are described in this section. All the advantages of Type-2 Fuzzy theory and FOCs were taken into account when developing the OH-FO-T2F-PID regulator. This typical control scheme offers many advantages over traditional Type-2 Fuzzy based PID regulator as presented in reference<sup>45</sup>. Figure 2 depicts the main layout of the closed-loop block diagram of the suggested OH-FO-T2F-PID regulator. In this regulator, the inputs to the Type-2 Fuzzy regulator are the scaled version of the error signal E(t) and the scaled version of the FO derivative of the error signal DE(t) with order  $\mu$ .

The output signal UT2-FLC(t) of the Type-2 Fuzzy regulator is multiplied by the scaling coefficient  $G_{PD}$ , and its fractional integral with order multiplied by the scaling coefficient  $G_{PI}$  and then summed to provide the final regulator output  $\tau(t)$ . Thus, the final control signal generated by the suggested regulator can be represented as follows:

$$\tau(t) = u_{FO-T2F-PID}(t) = G_{PI} \frac{U_{T2-FLC}^{-\lambda}(t)}{dt^{-\lambda}} + G_{PD} u_{T2-FLC}(t)$$
 (5)

where UT2-FLC(t) is the output of the Type 2 FLC, which is given as follows:

$$U_{T2-FLC}(t) = \zeta \left( G_{E}e(t), \quad G_{DE} \frac{d^{\mu}e(t)}{dt^{\mu}} \right)$$
 (6)

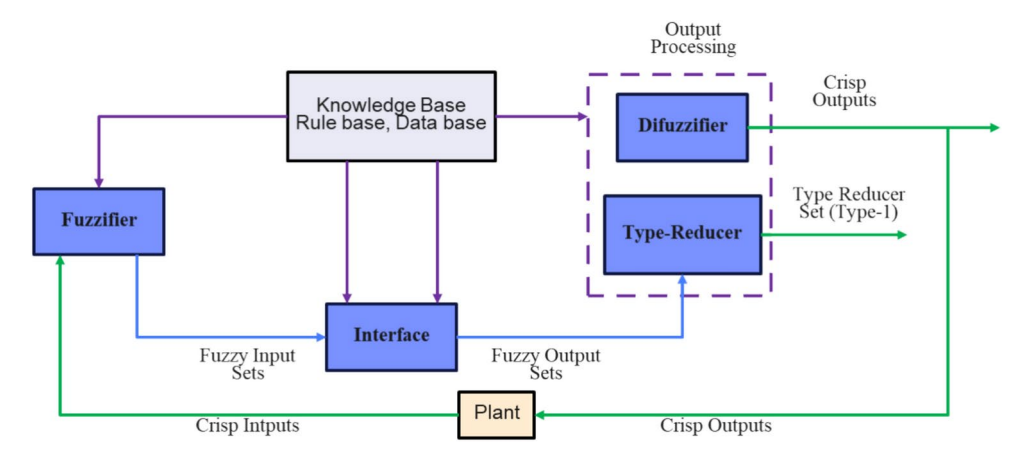


Fig. 3. Block representation of a Type-2 FLC.

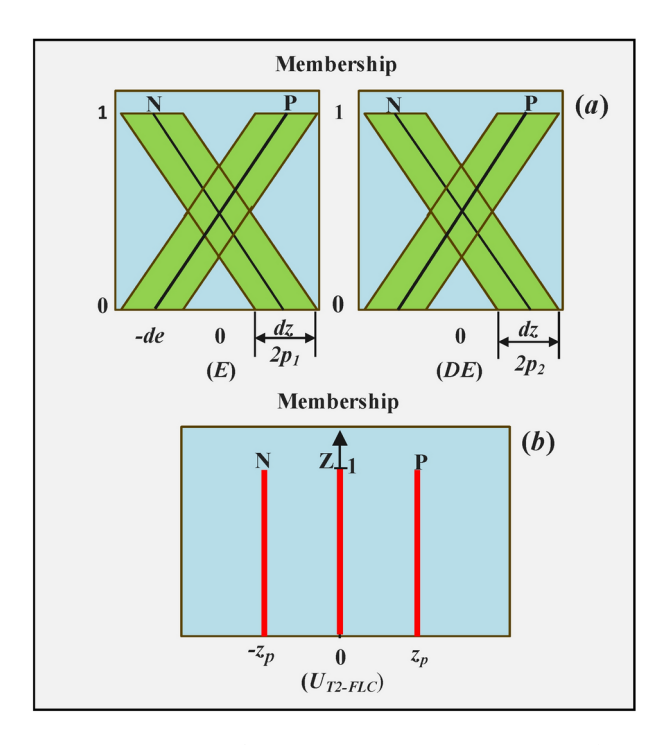


Fig. 4. Primary MFs for Fuzzy-2 system: (a) Inputs (E) and (DE), (b) Output (UT2-FLC).

where  $\zeta$  is a fuzzy-2 function. e(t) represents the difference between the reference liquid level  $h_d(t)$ , and the measured liquid level h(t).

It is worth noting that the Type 2 FLC serves as the basis for the suggested regulator, which is responsible for generating the main control action of OH-FO-T2F-PID regulator. The five basic components of a Type 2 FLC are the type reducer, the inference engine, the rule base, the fuzzifier, and the defuzzifier.

The configuration of the Type 2 fuzzy regulator is identical to that of the Type 1 fuzzy regulator, with the addition of a "Type Reducer" component to the output-processing unit<sup>45</sup>. Figure 3 displays a block representation of a Type 2 FLC.

For Type 2 fuzzy regulator output generation, a fuzzy rule base has been decided based on the liquid level control problem for the considered QTS. The input to the Type 2 fuzzy regulator is "E" and "DE", while the instantaneous control output isUT2-FLC. It is worth mentioning here that the UFO-T2F-PI and UFO-T2F-PD outputs of the Type 2 fuzzy regulator correspond to the Fuzzy-2-PI and the Fuzzy-2-PD control signals, respectively. The unique feature of the designed OH-FO-T2F-PID regulator is its ease of implementation as only two membership functions for the input linguistic variables are taken into account as illustrated in Fig. 4a, which greatly reduces the number of rules. In Fig. 4a, the shifts  $p_1$  and  $p_2$  present the footprint of uncertainty (FOU) of

the primary membership degree. It is possible to calculate the upper and lower boundaries of error (*E*) primary MFs for positive fuzzy sets using the following equations:

$$\overline{\mu}_{E}^{\tilde{P}} = \begin{cases}
0 & if \quad (E \le -dz + p_1) \\ \frac{E + dz + p_1}{2dz} & if \quad (-dz + p_1 < E < dz - p_1) \\
1 & if \quad (E \ge -dz + p_1)
\end{cases}$$
(7)

$$\underline{\mu}_{E}^{\tilde{P}} = \begin{cases} 0 & if \quad (E \le -dz + p_{1}) \\ \frac{E + dz - p_{1}}{2dz} & if \quad (-dz + p_{1} < E < dz - p_{1}) \\ 1 & if \quad (E \ge -dz + p_{1}) \end{cases}$$
(8)

In addition, it is possible to calculate the upper and lower boundaries of error (*E*) primary MFs for negative fuzzy sets using Eqs. (9) and (10):

$$\overline{\mu}_{E}^{\tilde{N}} = \begin{cases}
1 & if \quad (E \le -dz + p_{1}) \\
\frac{-E + dz + p_{1}}{2dz} & if \quad (-dz + p_{1} < E < dz + p_{1}) \\
0 & if \quad (E \ge dz + p_{1})
\end{cases}$$
(9)

$$\underline{\mu}_{E}^{\tilde{N}} = \begin{cases}
1 & if \quad (E \le -dz - p_1) \\
\frac{-E + dz - p_1}{2dz} & if \quad (-dz - p_1 < E < dz - p_1) \\
0 & if \quad (E \ge dz - p_1)
\end{cases}$$
(10)

The description of the upper and lower limits of the error deviation (DE) primary MFs in  $[-DE-p_2, -DE+p_2]$  are the same as Eqs. (7)–(10). On the other hand, two single-output MFs are formed, and positioned around zero at a distance " $z_p$ " from one another as shown in Fig. 4b.

In accordance with the two MFs defined for each linguistic variable, four fuzzy rules were developed, as follows:

Rule 1: if E is 'N' and DE is 'N', Then y1 = UT2-FLC is 'P'. Rule 2: if E is 'N' and DE is 'P', Then y2 = UT2-FLC is 'Z'. Rule 3: if E is 'P' and DE is 'N', Then y3 = UT2-FLC is 'Z'. Rule 4: if E is 'P' and DE is 'P', Then y4 = UT2-FLC is 'N'.

A  $2 \times 2$  rule base was created, as shown in Table 2, to achieve the best performance of the Fuzzy-2 system.

From fuzzy inference of interval Type-2 Fuzzy regulator, the fired membership degree of fuzzy rule is also an interval, the 4 rules interval are represented as Eqs. (11)-(14) using "product" operator:

$$\left[\underline{l}_{1}, \bar{l}_{1}\right] = \left[\underline{\mu}_{\tilde{A}_{i}}\left(E\right) \times \underline{\mu}_{\tilde{B}_{j}}\left(DE\right), \quad \overline{\mu}_{\tilde{A}_{i}}\left(E\right) \times \overline{\mu}_{\tilde{B}_{j}}\left(DE\right)\right] \tag{11}$$

$$\left[\underline{l}_{2}, \overline{l}_{2}\right] = \left[\underline{\mu}_{\tilde{A}_{i}}\left(E\right) \times \underline{\mu}_{\tilde{B}_{j+1}}\left(DE\right), \quad \overline{\mu}_{\tilde{A}_{i}}\left(E\right) \times \overline{\mu}_{\tilde{B}_{j+1}}\left(DE\right)\right] \tag{12}$$

$$\left[\underline{l}_{3}, \overline{l}_{3}\right] = \left[\underline{\mu}_{\tilde{A}_{i+1}}\left(E\right) \times \underline{\mu}_{\tilde{B}_{i}}\left(DE\right), \quad \overline{\mu}_{\tilde{A}_{i+1}}\left(E\right) \times \overline{\mu}_{\tilde{B}_{j}}\left(DE\right)\right] \tag{13}$$

$$\left[\underline{l}_{4}, \overline{l}_{4}\right] = \left[\underline{\mu}_{\tilde{A}_{i+1}}\left(E\right) \times \underline{\mu}_{\tilde{B}_{j+1}}\left(DE\right), \quad \overline{\mu}_{\tilde{A}_{i+1}}\left(E\right) \times \overline{\mu}_{\tilde{B}_{j+1}}\left(DE\right)\right] \tag{14}$$

 $[\underline{l}_i, \overline{l}_i]$  represent the lower and upper MF values of the interval Type-2 fuzzy sets. The fuzzy inference output UT2-FLC for the Type-2 FLS under consideration is determined using NT-type reduction techniques. Specifically, the output UT2-FLC is derived by averaging the upper and lower limits of the fired membership degrees for fuzzy rules, as shown in Eq. (15):

$$U_{T2-FLC} = \frac{\sum_{i}^{4} (\underline{l}_{i} + \bar{l}_{i}) y_{i}}{\sum_{i}^{4} (\underline{l}_{i} + \bar{l}_{i})}$$
(15)

Here is the final output of the OH-FO-T2F-PID regulator:

$$\tau(t) = G_{PD}u_{T2-FLC}(t) + G_{PI} \int u_{T2-FLC}(t) dt$$
 (16)

N	P
P	Z
Z	N
	P Z

Table 2. Rule base of Fuzzy-2 system.

It is also necessary to emphasize that the current article uses the Oustaloup approximation method to construct FO parts, which are necessary for the designed OH-FO-T2F-PID regulator to function in simulations or practical systems. As a result, it is easy to approximate the FO derivative operator  $s^{\theta}$  by constructing a higher-integer transfer function with many poles and zeros, as shown in Eq. (17):

$$s^{\theta} = G_f(s) = \alpha \prod_{k=-\varphi}^{\varphi} \frac{s + \omega_{z,k}}{s + \omega_{p,k}}$$
(17)

In Eq. (17)  $\alpha$  is the filter gain, where  $\omega_{z,k}$  and  $\omega_{p,k}$  are frequency bands, and can be computed using the following formulas<sup>46</sup>:

$$\omega_{z,k} = \omega_l \left(\frac{\omega_h}{\omega_l}\right)^{\frac{\alpha + \varphi + 0.5(1 - \theta)}{2\varphi + 1}} \tag{18}$$

$$\omega_{p,k} = \omega_l \left(\frac{\omega_h}{\omega_l}\right)^{\frac{\alpha + \varphi + 0.5(1 + \theta)}{2\varphi + 1}} \tag{19}$$

$$\alpha = \omega_h^{\theta} \tag{20}$$

where the approximation order is represented by  $(2\varphi + 1)$ . In this case, a fifth order filter with a suitable frequency range of  $\omega = [0.01, 100]$  rad/s is considered. For the sake of keeping the paper brief, an extensive overview of the FO calculus implementation is not included here.

In the next section, we will focus on adjusting the fractional derivative of the error and the Type 2 FLC outputs, while the MFs structure and the rule base stay in their initial form. Adjustable parameters like GE,  $G_{DE}$ ,  $G_{PD}$ ,  $G_{PP}$ , A, and  $\mu$  can significantly improve the performance of QTS.

#### Hybridized algorithm for regulator parameter tuning

This section presents a full discussion of the newly developed hAGWOCS algorithm as well as descriptions of the AGWO, CS, and the cost functions.

#### Overview of GWO algorithm

This approach was first introduced by Mirjalili et al. in 2014<sup>47</sup>.GWO is one of the newly recommended optimization methods, which is derived by the hunting mechanism and the hierarchy of grey wolves pack<sup>45</sup>. GWO consists of three essential points:

- Pursuing and getting close to the intended victim.
- Surrounding and restricting her movement.
- Chasing the victim.

Grey wolves hunt in groups according to a strict social order. The top group leader, known as  $(\alpha)$  wolf, is followed by  $(\beta)$  wolf,  $(\delta)$  wolf is the executor of  $(\beta)$  and  $(\delta)$  wolves, and the other internally balanced group of wolves is known as the  $(\omega)$  wolves. Figure 5 illustrates the hierarchy of gray wolves.

The following equation describes the actions of a pack of wolves surrounding a victim<sup>45</sup>:

$$\vec{V}\left(k+1\right) = \vec{V}_p\left(k\right) - \vec{P} \cdot \left| \vec{L} \cdot \vec{V}_p\left(k\right) - \vec{V}\left(k\right) \right| \tag{21}$$

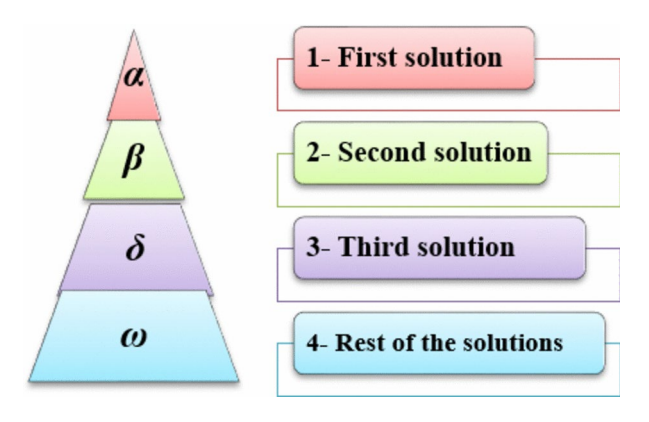


Fig. 5. Block representation of a Type-2 FLC.

 $\vec{V}_p(k)$  and  $\vec{V}(k)$  correspond to the position vectors of the victim and the wolf at iteration k, respectively. The coefficients vectors and are computed by Eq. (22) and (23):

$$\vec{P} = 2 \cdot \vec{\eta} \cdot \vec{q}_1 - \vec{\eta} \tag{22}$$

$$\vec{L} = 2 \cdot \vec{q}_2 \tag{23}$$

The vector  $(\vec{\eta})$  is computed as follows, taking into account two random vectors,  $(\vec{q}_1)$  and  $(\vec{q}_2)$ , having values in the interval [0, 1]:

$$\vec{\eta}(k) = 2 - \frac{2 \cdot k}{Itermax} \tag{24}$$

where *Itermax* indicates the max iteration. Equation (23) gives the updated location of each member of the community:

$$\vec{V}(k+1) = \frac{\vec{V}_1(k) + \vec{V}_2(k) + \vec{V}_3(k)}{3}$$
(25)

where  $\vec{V}_1(k)$ ,  $\vec{V}_2(k)$ , and  $\vec{V}_3(k)$  are calculated as follows:

$$\vec{V}_{1}\left(k\right) = \vec{V}_{\alpha}\left(k\right) - \vec{P}_{1} \left| \vec{L}_{1} \cdot \vec{V}_{\alpha}\left(k\right) - \vec{V}\left(k\right) \right| \tag{26}$$

$$\vec{V}_{2}(k) = \vec{V}_{\beta}(k) - \vec{P}_{2} \left| \vec{L}_{2} \cdot \vec{V}_{\beta}(k) - \vec{V}(k) \right|$$
(27)

$$\vec{V}_{3}(k) = \vec{V}_{\delta}(k) - \vec{P}_{3} \left| \vec{L}_{3} \cdot \vec{V}_{\delta}(k) - \vec{V}(k) \right|$$
(28)

For all three wolves, the optimal places in each iteration are vectors  $\vec{V}_{\alpha}(k)$ ,  $\vec{V}_{\beta}(k)$ , and  $\vec{V}_{\delta}(k)$ , respectively. Assuming that the coefficient vectors  $(\vec{P}_1)$ ,  $(\vec{P}_2)$ , and  $(\vec{P}_3)$  are calculated using Eq. (22), and the coefficient vectors  $(\vec{L}_1)$ ,  $(\vec{L}_2)$ , and  $(\vec{L}_3)$  are calculated using Eqs. (23). A more comprehensive explanation of GWO can be found in referce<sup>47</sup>. The vector  $(\vec{\eta})$  is a fundamental control parameter in the standard GWO, determining the exploitation and exploration stages of the entire process. When the decay rate of vector  $\eta$  is slow, the exploration ratio of the grey wolf will be greater than the development ratio, which is suitable for global search. In contrast, it is suitable for local search to establish equilibrium between exploitation and exploration. Qais<sup>48</sup> developed an enhanced version of GWO called AGWO, which improves the GWO exploration process without losing its robustness and simplicity. In this article, to provide enough exploration durations throughout the first phase of a typical GWO, the vector  $(\vec{\eta})$  is modified according to Eq. (29):

$$\vec{\eta}(k) = 2 - \frac{\cos(rand) \cdot k}{Itermax} \tag{29}$$

This approach helps to find the best value more precisely and prevents falling into the trap of local optimum by performing an exhaustive search over the entire possible space. The hunting behavior in the suggested AGWO will rely solely on  $(\alpha)$  and  $(\beta)$ , as shown in Eqs. (30)–(32):

$$\vec{V}_{\alpha}(k) = \left| L_1 \vec{V}_{\alpha}(k) - \vec{V}(k) \right|, \quad \vec{V}_{\beta}(k) = \left| L_2 \vec{V}_{\beta}(k) - \vec{V}(k) \right| \tag{30}$$

$$\vec{V}_{1}(k) = \vec{V}_{\alpha}(k) - \vec{P}_{1}\vec{V}_{\alpha}(k), \quad \vec{V}_{2}(k) = \vec{V}_{\beta}(k) - \vec{P}_{2}\vec{V}_{\beta}(k)$$
 (31)

$$\vec{V}(k+1) = \frac{\vec{V}_1(k) + \vec{V}_2(k)}{2}$$
(32)

#### Overview of CS algorithm

The CS optimizer was first introduced in 2009 by Yang et al.<sup>49</sup>. CS, which mimics the parasitizing behavior of cuckoo breeding to solve optimization issues. The CS solution is equivalent to the cuckoo egg. In general, CS are designed based on the following three guidelines<sup>50</sup>:

- Cuckoos place only one egg at a time.
- Cuckoos deposit their eggs randomly in a selected nest.
- Only the finest nests with high quality eggs will inherit to the future generation.

The total number of available host nests is limited. Figure 6 illustrates the processes of CS algorithm, which is drawn by the authors.

Equation (33) shows how the cuckoo updates its position by searching for a new nest site<sup>51</sup>:

$$D(k+1) = D(k) - \Gamma(D(k) - D_g(k)) \oplus levy(\varepsilon)$$

$$= D(k) + \frac{0.01\sigma}{|\varphi|^{1/\varepsilon}} (D(k) - D_g(k))$$
(33)

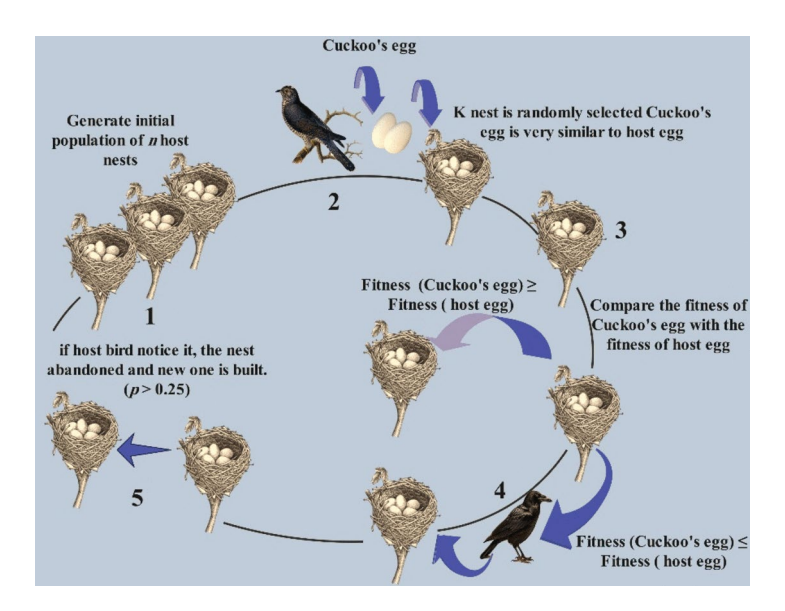


Fig. 6. Processes of CS algorithm.

The preceding formula has two unique solutions, D(k+1) and D(k), determined via a random walk.  $\oplus$  denotes point-to-point multiplication. The step size is adjusted by a parameter  $\Gamma > 0$ , and  $D_g(k)$  is the global optimal solution. Both  $(\sigma)$  and  $(\varphi)$  are arbitrary numbers, respectively.  $Levy(\varepsilon)$  is a random variable that follows the Levy distribution, as shown in Eq. (34):

$$levy(\varepsilon) \approx t^{-\varepsilon}, \quad 1 < \varepsilon \le 3$$
 (34)

In addition, CS replaces the found nests with probability  $(P_a)$  using the discovery operator as shown in Eq. (35)<sup>52</sup>:

$$D(k) = \begin{cases} D(k) + rand \cdot (D_j(k) - D_m(k)), & if P > P_a \\ D(k), & else \end{cases}$$
(35)

where  $P_a \in [0, 1]$  is an arbitrary integer,  $D_i$  and  $D_m$  are the possible solutions.

#### Overview of proposed hAGWOCS algorithm

Relevant algorithms like CS and AGWO are not recommended when the problem involves large dimensions with more fitness evaluations or vice versa. Therefore, in this article the CS algorithm is combined with the AGWO method to obtain higher optimization performance. The suggested hybrid variant is named hAGWOCS algorithm. It resembles the AGWO, except the modifications of the location vector of the searching agents in the AGWO are updated by the CS algorithm.

In this regard, the location update formula of CS is utilized to adjust the locations, convergence accuracy and velocity of the gray wolf agent ( $\alpha$ ) for the objective of maintaining a correct equilibrium between exploitation and exploration and improving the convergence speed of AGWO algorithm, while the rest of the AGWO operations are the same. Consequently, Eq. (36) provides the updated position vector D(k+1) for the proposed hAGWOCS algorithm:

$$D(k+1) = D(k) + \frac{0.01\sigma}{|\varphi|^{\frac{1}{\varepsilon}}} \left( D(k) - D_g(k) \right)$$
(36)

The procedures to take when developing the proposed hAGWOCS method are as follows:

Step 1: Determine the initial number of gray wolves using the following equation:

$$\vec{M}_i = \{\vec{M}_1, \vec{M}_2, \dots, \vec{M}_f, \dots, \vec{M}_k\}; \quad 1 < f \le \Omega$$
 (37)

where  $\Omega$  represents all the community's solutions.

*Step 2:* Calculate the fitness values of each agent and arrange them. AGWO utilizes two best solutions, ( $\alpha$ ) which is the first finest agent, and ( $\beta$ ) which is the second finest search agent.

**Step 3:** Verify if  $k < \text{Iter\_max}$ . If so, go to:

Update the current search agent position based on the encirclement behavior, as expressed by the flowing equation:

$$\vec{M}_{i}(k+1) = \vec{M}_{i}(k) - \vec{P}_{i} \cdot \vec{M}_{i}(k)$$
(38)

Calculate the overall best position for the current iteration by Eq. (39):

$$\vec{M}_{o}(k+1) = \frac{\vec{M}_{1}(k) + \vec{M}_{2}(k) + \vec{M}_{3}(k)}{3}$$
(39)

The aforementioned equation is changed by adding another term  $\vec{M}_4$  (k) to the numerator, as seen in Eq. (40), to provide the location update in the suggested hAGWOCS method:

$$\vec{M}_{o}(k+1) = \frac{\vec{M}_{1}(k) + \vec{M}_{2}(k) + \vec{M}_{3}(k) + \vec{M}_{4}(k)}{4}$$
(40)

 $\vec{M}_4$  (k) represents the location vector, which is determined by the CS method as follow:

$$\vec{M}_{4}(k) = \vec{M}_{o}(k) + \Gamma \oplus levy(\varepsilon)$$
(41)

where  $\vec{M}(k)$  denotes the location of the search agent at the present iteration, and  $\Gamma \in [0, 1]$  represents the step size. The term  $\vec{M}_4(k)$  improves the efficiency of the suggested hAGWOCS algorithm by allowing it to use Levy flight to explore the search space. Thus, the location of other agents around the prey will be randomly updated.

Step 4: Update the fitness value of all search agents;

Calculate the fitness of all updated search agents. The solution with the highest fitness value replaces the poorest solution, and thus the best solution is selected:

$$Iter = Iter + 1$$

*Step 5:* Continue repeating stages 2 through 5 until the maximum count, or "*Itermax*," is attained, where the best solution can be found so that the designed fitness aids in identifying the best solutions at both the lower and the upper limits. The flow diagram depicted in Fig. 7 describes the different steps involved in the suggested hAGWOCS algorithm.

#### Statistical evaluation of the proposed hAGWOCS method Quantitative analysis of hAGWOCS method

This subsection aims to use the CEC2005 standard functions<sup>53</sup> to evaluate the performance of the suggested hAGWOCS method. The CEC2005 benchmark functions were considered, including unimodal, multi-modal and fixed-dimensional benchmark problems. Table 3 outlines the characteristics of the Benchmark test functions employed in this study. Statistical evaluation of the hAGWOCS method from standard function tests over 30 independent runs was compared to those with regular GWO<sup>30</sup> method for a 30 search agents and 500 generations. The minimum, maximum, mean, standard deviations (STD) and computational time (CPU time/s) of both algorithms for the first set of benchmark functions are summarized in Table 4.

It is clear from the obtained values that the suggested hAGWOCS outperforms GWO method for functions F1, F2, F3, F4, F6 and F7, in which the obtained STD values with the suggested hAGWOCS are equal/close to 0 or far smaller than the mean values. The GWO method performance in function F5 is better than the suggested hAGWOCS method. In addition, GWO has high computational efficiency compared to the hAGWOCS method and has several functions with less than 10 s.

Table 5 displays the statistical outcomes of the second set of benchmark functions using the suggested hAGWOCS and GWO methods. It is analyzed from Table 5 and found that suggested hAGWOCS still produces optimal outcomes or maintains good performance in terms of mean, minimum, maximum, and standard deviation value in functions F8-F13, while providing worse results in computational time as compared to GWO method.

Table 6 provides an explanation of the third set of benchmark functions utilizing hAGWOCS and GWO methods. Across individual benchmark functions, the recommended hAGWOCS consistently outperformed its counterpart, providing lower average and standard deviation values. It is worth mentioning that for functions such as F15–F20 and F23, the suggested hAGWOCS method showed the best results, demonstrating its robustness. In addition, for function F15, the suggested hAGWOCS method maintained its dominance.

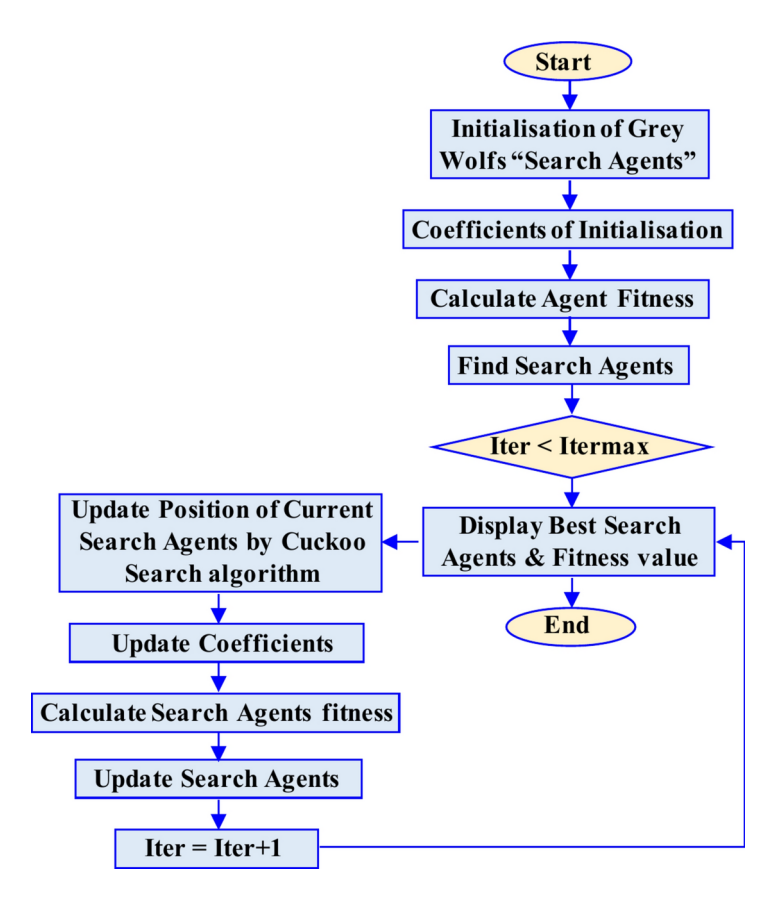


Fig. 7. Flowchart of the proposed hAGWOCS method.

Overall, the statistical findings illustrate the capacity and effectiveness of the suggested hAGWOCS method in finding optimal solutions more consistently than the standard GWO method.

#### hAGWOCS versus 23 representative optimization methods

To fully validate the capabilities of the suggested hAGWOCS method, 23 state-of-the-art and outstanding optimization methods were utilized to compare with hAGWOCS, including PSO $^{54}$ , gravitational search optimizer (GSO) $^{55}$ , differential evolution optimizer (DEO) $^{56}$ , fruit fly optimizer (FFO) $^{57}$ , ant lion algorithm (ALA) $^{58}$ , symbiotic organisms search optimizer (SOSO) $^{59}$ , bat optimizer (BO) $^{60}$ , flower pollination optimizer (FPO) $^{61,62}$ , cuckoo search (COS) $^{32}$ , firefly optimizer (FO) $^{63}$ , genetic optimizer (GO) $^{64}$ , grasshopper optimization algorithm (GOA) $^{65}$ , Moth-flame algorithm (MFO) $^{66}$ , multiverse algorithm (MVA) $^{67}$ , Dragonfly optimizer (DO) $^{68}$ , binary bat optimizer (BBO) $^{69}$ , Biogeography algorithm (BA) $^{70}$ , binary gravitational search optimizer (BGSO) $^{71}$ , sine cosine optimizer (SCO) $^{72}$ , salp swarm optimizer (SSO) $^{73}$ , whale optimization algorithm (WOA) $^{74}$ , binary moth flame algorithm (BMFA1 and BMFA2) $^{75}$ , and Enhanced grey wolf optimizer (E-GWO) $^{76,77}$ . Table 7 presents the essential information of the compared optimization methods for the first set of benchmark functions.

Table 8 provides the comparative findings for the second set of benchmark functions, which relate to different modern heuristic search methods.

The comparison results between hAGWOCS and 23 modern heuristic search methods for the third set of benchmark functions are presented in Tables 9 and 10.

From the previous results among 23 selected methods, we can see that suggested hAGWOCS outperforms thirteen compared methods in terms of accuracy (ALA, SOSO, BO, FPO, CS, FO, GO, GOA, MVA, DO, BBO, WOA, and E-GWO), and is only worse than ten compared methods.

#### Qualitative analysis of hAGWOCS method

Figure 8 provides the qualitative analysis metrics of hAGWOCS and standard GWO methods, including the shapes of tested functions, the search history, average fitness history, and convergence curve. For simplicity, we focus on six classical benchmark functions (F4, F7, F8, F9, F19, and F23), including unimodal, multi-modal, and fixed-dimensional functions. In the second column of Fig. 8, the search histories show all the positions of starfish during the optimization process, illustrating that the positions of starfish are widely distributed in the entire search space, with more in the areas that promise the best solution during the exploration phase. The third and fourth columns show the average fitness values and convergence curves of hAGWOCS method, demonstrating its good convergence capability in solving unimodal, multi-modal and fixed-dimensional functions. In conclusion, the exploration and exploitation of hAGWOCS method are illustrated by the qualitative analysis.

Type	Definition	S	p	$F_{opt}$
	$f_1(X) = \sum_{i=1}^d x_i^2$	[-100, 100] <sup>d</sup>	30	0
	$f_2(X) = \sum_{i=1}^{d}  x_i  + \prod_{i=1}^{d}  x_i $	[-10, 10] <sup>d</sup>	30	0
	$f_3(X) = \sum_{i=1}^d \left(\sum_{j=1}^i x_j\right)^2$	[-100, 100] <sup>d</sup>	30	0
Unimodal test functions	$f_4(X) = max\{ x_i , 1 \le i \le d\}$	[-100, 100] <sup>d</sup>	30	0
	$f_5(X) = \sum_{i=1}^{d-1} \left[ 100 \left( x_{i+1} - x_i^2 \right)^2 + (x_i - 1)^2 \right]$	[-30, 30] <sup>d</sup>	30	0
	$f_6(X) = \sum_{i=1}^d ([x_i + 0.5])^2$	[-100, 100] <sup>d</sup>	30	0
	$f_{7}(X) = \sum_{i=1}^{d} ix_{i}^{4} + random[0, 1)$	[-1.28, 1.28] <sup>d</sup>	30	0
	$f_{8}\left(X\right) = \sum_{i=1}^{d} -x_{i} \sin\left(\sqrt{\left x_{i}\right }\right)$	[-500, 500] <sup>d</sup>	30	- 418.982*d
	$f_9(X) = \sum_{i=1}^{d} \left[ x_i^2 - 10\cos(2\pi x_i) + 10 \right]$	[-5.12, 5.12] <sup>d</sup>	30	0
	$f_{10}\left(X\right) = -20exp\left(-0.2\sqrt{\frac{1}{30}\sum_{i=1}^{d}x_{i}^{2}}\right) - exp\left(\frac{1}{30}\sum_{i=1}^{d}\cos2\pi x_{i}\right) + 20 + e  \left[-32,32\right]^{d}$		30	0
	$f_{11}(x) = \frac{1}{4000} \sum_{i=1}^{d} x_i^2 - \prod_{i=1}^{d} \cos\left(\frac{x_i}{\sqrt{x_i}}\right) + 1$	[-600, 600] <sup>d</sup>	30	0
Mulumodal test functions	$f_{12}(x) = \frac{\pi}{d} \left\{ 10\sin(\pi y_1) + \sum_{i=1}^{d-1} (y_1 - 1)^2 \left[ 1 + 10\sin^2(\pi y_{i+1}) \right] + \sum_{i=1}^{d} u(x_i, 10, 100, 4) \right\}$	[-50, 50] <sup>d</sup>	30	0
	$f_{13}(x) = 0.1 \left\{ sin^{2} (3\pi x_{i}) + \sum_{i=1}^{d} (x_{i} - 1)^{2} \left[ 1 + sin^{2} (3\pi x_{i} + 1) \right] + (x_{n} - 1)^{2} \left[ sin^{2} (2\pi x_{n}) \right] \right\} + \sum_{i=1}^{d} u(x_{i}, 5, 100, 4)$	[-50, 50] <sup>d</sup>	30	0
Continued		-		

Type	Definition	S	р	Fopt
	$f_{14}\left(X\right) = \left[\frac{1}{500} + \sum_{j=1}^{25} \frac{1}{j + \sum_{i=1}^{2} \frac{1}{\left(x_{i} - a_{ij}\right)^{6}}}\right]^{-1}$	[-65.53, 65.53] <sup>d</sup> 2	2	1
	$f_{15}\left(X\right) = \sum_{i=1}^{11} \left[ a_i - \frac{x_i \left(b_i^2 + b_i x_2\right)}{b_i^2 + b_i x_3 + x_3} \right]^2$	[-5,5] <sup>d</sup>	4	0.0003
	$f_{16}(X) = 4x_1^2 - 2.1x_1^4 + \frac{1}{3}x_1^6 + x_1x_2 - 4_2^2 + 4_2^4$	[-5,5] <sup>d</sup>	2	-1.0316
	$f_{17}(X) = \left(x_2 - \frac{5.1}{4\pi^2}x_1^2 + \frac{5}{\pi}x_1 - 6\right)^2 + 10\left(1 - \frac{1}{8\pi}\right)\cos x_i + 10$	$[-5, 10]^*[0, 15]$	2	0.398
Multimodal test functions with fixed dimension	$f_{18}(X) = \left[1 + (x_1 + x_2 + 1)^2 \left(19 - 14x_1 + 3x_1^2 - 14x_2 + 6x_1x_2 + 3x_2^2\right)\right]$ $* \left[30 + (2x_1 - 3x_2)^2 * \left(18 - 32x_1 + 12x_1^2 + 48x_2 - 36x_1x_2 + 27x_2^2\right)\right]$	[-5, 5] <sup>d</sup>	7	3
	$f_{19}(X) = -\sum_{i=1}^{4} c_i \exp\left[-\sum_{j=1}^{d} a_{ij} (x_j - p_{ij})^2\right]$	[0,1] <sup>d</sup>	3	-3.86
	$f_{20}(X) = -\sum_{i=1}^{4} \dot{c}_i exp\left[-\sum_{j=1}^{d} \dot{a}_{ij} (x_j - \dot{p}_{ij})^2\right]$	[0, 1] <sup>d</sup>	9	-3.32
	$f_{21}(X) = -\sum_{i=1}^{5} [(x - a_i)(x - a_i)^T + c_i]^{-1}$	$[0, 10]^d$	4	-10.1532
	$f_{22}(X) = -\sum_{i=1}^{7} [(x - a_i)(x - a_i)^T + c_i]^{-1}$	[0, 10] <sup>d</sup>	4	-10.4028
	$f_{23}(X) = -\sum_{i=1}^{10} \left[ (x - a_i) (x - a_i)^T + c_i \right]^{-1}$	$[0, 10]^d$	4	-10.5363

 Table 3. Details of the CEC2005 benchmark functions.

	Parameters	S			
Benchmark functions	Mean	Minimum	Maximum	STD	CPU time/s
(a) GWO method					
F1	0	0	0	0	6.994336
F2	0	0	0	0	7.052458
F3	0.000018	0	0.000150	0.000036	12.625437
F4	0.000001	0	0.000005	0.000001	6.788589
F5	27.014286	25.391669	28.560246	0.792544	7.649939
F6	0.804452	0.245737	1.499982	0.365254	6.860489
F7	0.002324	0.000464	0.007825	0.001543	10.195327
(b) hAGWOCS method					
F1	0	0	0	0	57.048718
F2	0	0	0	0	73.943569
F3	0.000004	0	0.000065	0.000014	85.442414
F4	0	0	0.000001	0	94.131331
F5	27.370193	26.115530	28.738033	0.711924	77.569280
F6	0.773325	0.000083	1.996052	0.408231	64.066145
F7	0.002147	0.000216	0.005093	0.001183	56.830416

**Table 4**. (a) Statistical outcomes of GWO in solving F1–F7, (b) statistical outcomes of hAGWOCS in solving F1–F7.

	Parameters				
Benchmark functions	Mean	Minimum	Maximum	STD	CPU time/s
(a) GWO method					
F8	- 5787.771936	-8024.1072	-2768.54088	1251.334052	7.747784
F9	2.022602	0	12.579128	3.476486	6.978757
F10	0	0	0	0	7.053411
F11	0.002304	0	0.016191	0.005280	7.562258
F12	0.054082	0.006977	0.129327	0.030135	16.459652
F13	0.655472	0.100965	1.029676	0.237728	16.342275
(b) hAGWOCS method					
F8	-11,271.110227	-12,557.323	-6693.28338	1224.552715	50.105055
F9	1.318777	0	6.333866	2.103797	76.055162
F10	0	0	0	0	98.658536
F11	0.006341	0	0.062605	0.012583	94.023724
F12	0.040212	0.016262	0.104982	0.021329	80.954757
F13	0.627942	0.205084	1.148275	0.235043	87.323335

**Table 5**. (a) Statistical outcomes of GWO in solving F8–F13, (b) statistical outcomes of hAGWOCS in solving F8–F13.

The suggested hAGWOCS method achieves the balance between the exploration and exploitation, which can ensure the searching capacity and the convergence during the optimization process.

#### Cost function for tuning the proposed OH-FO-T2F-PID regulator

As discussed in the previous section, the proposed OH-FO-T2F-PID regulator can be optimal when its control gains are tuned optimally by minimizing the fitness function. A fitness function in multi-objective optimization process is the weighted sum of two or more cost functions. During the optimization process, it is necessary to minimize the error index as well as the control inputs. In this paper, the performance indicator has been taken into consideration as follows:

$$J = ISCS + ITAE = \int_{0}^{T_{sim}} \tau^{2}(t) dt + \int_{0}^{T_{sim}} t |E(t)| dt$$
 (42)

In this case,  $T_{sim}$  stands for computational time,  $\tau(t)$  represents the control input, and ITAE is the integral time absolute error. ISCS is the integral of the squared control signal. This fitness function is suitably reduced when the suggested OH-FO-T2F-PID regulator approaches near-optimal gain values. Thus, the considered hAGWOCS

	Parameter	s			
Benchmark functions	Mean	Minimum	Maximum	STD	CPU time/s
(a) GWO method					
F14	3.714756	0.998004	12.67050	3.486832	19.207965
F15	0.003812	0.000307	0.020363	0.007535	1.666219
F16	-1.03162	-1.031628	-1.03162	0	1.294090
F17	0.397905	0.397887	0.398326	0	1.042838
F18	3.000042	3	3.000282	0.000068	0.976506
F19	-3.86165	-3.862782	-3.85489	0.002191	1.715316
F20	-3.26480	-3.321992	-3.07850	0.075802	2.339533
F21	-9.81439	-10.15303	-5.09862	1.281744	2.174023
F22	- 9.96947	-10.40271	-2.76575	1.670664	2.458147
F23	- 9.99386	-10.53636	-2.42164	2.058353	2.899639
(b) hAGWOCS method			,		
F14	4.581569	0.998004	12.67050	4.614445	95.005466
F15	0.000328	0.000307	0.000471	0.000041	19.226762
F16	-1.03162	-1.031628	-1.03162	0	16.451468
F17	0.397889	0.397887	0.397898	0.000002	16.039501
F18	3.000049	3	3.000140	0.000047	16.273713
F19	-3.86271	-3.862781	-3.86226	0.000100	17.920867
F20	-3.31405	-3.321993	-3.20295	0.030191	21.400611
F21	-8.71615	-10.15290	-2.68251	2.455752	19.734806
F22	- 9.46860	-10.40240	-3.61043	2.134653	20.553430
F23	- 9.63668	-10.53602	-5.12845	2.042330	21.321838

**Table 6**. (a) Statistical outcomes of GWO in solving F14–F23, (b) statistical outcomes of hAGWOCS in solving F14–F23.

algorithm minimizes the cost function (*J*) to produce optimally tuned scaling factors for the inputs/outputs, as well as fractional integral–differential orders for the suggested OH-FO-T2F-PID regulator with low control signal and error-index. So, the design problem for QTS can be described by the following restricted optimization problem, where the constraints are the gains limits of the suggested OH-FO-T2F-PID regulator:

$$Minimize J(x) = (G_E, G_{DE}, G_{PD}, G_{PI}, \lambda, \mu) \in \Re^6$$

$$Subject to: \begin{cases} G_{E,min} \leq G_E \leq G_{E,max} \\ G_{DE,min} \leq G_{DE} \leq G_{DE,max} \\ G_{PD,min} \leq G_{PD} \leq G_{PD,max} \\ G_{PI,min} \leq G_{PI} \leq G_{PI,max} \\ \lambda_{min} \leq \lambda \leq \lambda_{max} \\ \mu_{min} \leq \mu \leq \mu_{max} \end{cases}$$

In this case, the limits of  $G_{E'}$ ,  $G_{DE'}$ ,  $G_{PD'}$  and  $G_{Pl}$  are defined in the range [0, 10]. The search bounds of the optimization problem are determined by the gain range of the FO-T2F-PID regulator, which limits the cost function (42). The optimizations gains' maximum and minimum bounds of the FO-T2F-PID regulator are summarized in Table 11.

Figure 9 depicts a block diagram of the optimization process for the OH-FO-T2F-PID regulator using the proposed hAGWOCS algorithm. Here, MATLAB software environment was utilized to determine the best optimum values for each of the six regulator gains.

The hAGWOCS technique has been run for a sufficient number of iterations to guarantee that it converges to the optimal point. Figure 10 displays the convergence profile of the suggested hAGWOCS method, which outperforms its competitor by reaching the optimal values in 117 iterations.

#### Simulation tests

Simulations performed under the different transient and dynamic scenarios confirm the efficiency and effectiveness of the designed OH-FO-T2F-PID regulator. The parameters listed in Table 1 were exploited in the QTS built-in model included in the MATLAB software environment. Tables 12, 13 and 14 summarize the optimal values for each regulators utilized in the configuration model under study. The following tests can help clarify the simulation results.

#### Test 1, tracking performance under step-point reference

In the first test, the reference level was fixed at 8 cm for 0 to 100 s, and then the second reference level was fixed at 11 cm for 100 to 200 s, while the third reference level was fixed at 14 cm for 200 to 300 s and the final reference

		Benc	hmark f	unctions				
Algorithms	Parameters	F1	F2	F3	F4	F5	F6	F7
20251	Mean	0	0.04	70.13	1.09	96.72	0	012
PSO <sup>54</sup>	STD	0	0.05	22.12	0.32	60.12	0	0.04
2025	Mean	0	0.06	896.53	7.35	67.54	0	0.09
GSO <sup>55</sup>	STD	0	0.19	318.96	1.74	62.23	0	0.04
	Mean	0.01	0.01	0.01	0.01	0.1	0.01	0.01
DEO <sup>56</sup>	STD	1.01	1.01	1.01	1.01	1.01	1.01	1.01
	Mean	0.05	0.06	0.04	0.4	5.06	0.02	0.14
FFO <sup>57</sup>	STD	0.02	0.02	0.01	1.5	5.87	0	0.35
50	Mean	0.01	0.01	0	0.01	0.35	0.01	0
ALA <sup>58</sup>	STD	0.01	0	0.01	0.01	0.11	0.01	0.01
0.00050	Mean	0.06	0.01	0.96	0.28	0.09	0.13	0
SOSO <sup>59</sup>	STD	0.01	0	0.82	0.01	0.14	0.08	0
	Mean	1.77	1.33	1.12	1.19	1.33	1.78	1.14
BO <sup>60</sup>	STD	1.53	4.82	1.77	1.89	1.3	1.67	1.11
	Mean	0.01	0.01	0.01	0.01	0.78	0.01	0.01
FPO <sup>61,62</sup>	STD	0.01	0.01	0.01	0.01	0.37	0.01	0.01
	Mean	0	1.21	1.25	0.01	0.01	0.01	0.01
CS <sup>32</sup>	STD	0	1.04	1.02	0.01	0.01	0.01	0.01
	Mean	0.04	0.05	0.05	0.15	2.18	0.06	0
FO <sup>63</sup>	STD	0.01	0.01	0.02	0.03	1.45	0.01	0
	Mean	0.12	0.15	0.14	0.16	0.71	0.17	0.01
GO <sup>64</sup>	STD	0.13	0.05	012	0.86	0.97	0.87	0
	Mean	0.01	0.01	0.01	0.01	0.01	0.01	0.01
GOA <sup>65</sup>	STD	0.01	0.01	0.02	0.01	0.01	0.01	0.01
	Mean	0.01	0.01	0.01	0.07	27.87	3.12	0
MFO <sup>66</sup>	STD	0	0	0	0.4	0.76	0.53	0
	Mean	2.06	15.92	453.2	3.12	1272.1	1.29	0.05
MVA <sup>67</sup>	STD	0.65	44.75	177.1	1.58	1479.5	0.63	0.03
	Mean	0.03	0.01	0.01	0.01	7.6	0.01	0.01
$DO^{68}$	STD	0.01	0.01	0.01	0.01	6.79	0.01	0.01
	Mean	1.28	1.06	15.6	1.25	24.7	1.1	1.01
BBO <sup>69</sup>	STD	1.42	1.07	23.8	1.33	35.8	1.14	1.01
	Mean	6.52	0.2	16.7	2.8	87.6	7.96	0.01
BA <sup>70</sup>	STD	2.99	0.05	14.9	1.47	66.9	4.87	0.01
	Mean	85	1.19	458	7.35	3110	106	0.04
BGSO <sup>71</sup>	STD	48.7	0.23	275	2.25	2936	77.7	0.04
	Mean	0.01	0.23	0.06	0.1	0.01	0.01	0.00
SCO <sup>72</sup>	STD	0.01	0.01	0.14	0.58	0.01	0.01	0.01
	Mean	0.01	0.01	0.01	0.01	0.01	0.01	0.01
SSO <sup>73</sup>	STD		1	0.01	0.66	0.01	0.01	0.01
	Mean	0.01		696.73	70.69	139.15	0.01	0.01
WOA <sup>74</sup>		0.01	0.01	188.53		120.26		
	STD	0.01	0.01		5.28		0.01	0.05
BMFA1 <sup>75</sup>	Mean	0.01	0.01	0.01	0.04	3.14	0.01	0.01
	STD	0.01	0.01	0.01	0.09	2.22	0.01	0.01
BMFA2 <sup>75</sup>	Mean	0.01	0.01	0.01	0.05	3.46	0.01	0.01
	STD	0.01	0.01	0.01	0.1	2.25	0.01	0.01
E-GWO <sup>76,77</sup>	Mean	0	0	0.000018	0.000001	27.014286	0.804452	0.002324
	STD	0	0	0.000036	0.000001	0.792544	0.365254	0.001543
hAGWOCS	Mean	0	0	0.000004	0	27.370193	0.773325	0.002147
	STD	0	0	0.000014	0	0.711924	0.408231	0.001183

 Table 7. Comparison of uni-modal benchmark functions.

		Benchmark	functions				
Algorithms	Parameters	F8	F9	F10	F11	F12	F13
	Mean	-4840	46.7	0.28	0.01	0.01	0.01
PSO <sup>54</sup>	STD	1150	11.6	0.51	0.01	0.03	0.01
	Mean	-2820	26	0.06	27.7	1.8	5.9
GSO <sup>55</sup>	STD	493	7.47	0.24	5.04	0.95	7.13
	Mean	-11,100	69.2	0	0	0	0
DEO <sup>56</sup>	STD	575	38.8	0	0	0	0
	Mean	-12,600	0.05	0.02	0.02	0	0
FFO <sup>57</sup>	STD	52.6	0.01	0	0.02	0	0
	Mean	-1610	0	0	0.02	0	0
ALA <sup>58</sup>	STD	314	0	0	0.01	0	0
	Mean	-4.21	1.33	0	0.71	0.12	0.01
SOSO <sup>59</sup>	STD	0	0.33	0	0.91	0.04	0
	Mean	-1070	1.23	0.13	1.45	0.4	0.39
BO <sup>60</sup>	STD	858	0.69	0.04	0.57	0.99	0.12
	Mean	-1840	0.27	0.01	0.09	0	0
FPO <sup>61,62</sup>	STD	50.4	0.07	0.01	0.04	0	0
	Mean	-2090	0.13	0	0.12	0	0
CS <sup>32</sup>	STD	0.01	0	0	0.05	0	0
	Mean	-1250	0.26	0.17	0.1	0.13	0
FO <sup>63</sup>	STD	353	0.18	0.05	0.02	0.26	0
	Mean	-2090	0.66	0.96	0.49	0.11	0.13
GO <sup>64</sup>	STD	2.47	2.47	0.81	0.22	0.07	0.07
	Mean	1	0	0.1	0	0	0
GOA <sup>65</sup>	STD	0	0	0	0	0	0
	Mean	-5080	0	7.4	0	0.34	1.89
MFO <sup>66</sup>	STD	696	0	9.9	0	0.22	0.27
	Mean	-11,700	118	4.07	0.94	2.46	0.22
MVA <sup>67</sup>	STD	937	39.3	5.5	0.06	0.79	0.09
	Mean	-2860	16	0.23	0.19	0.03	0
DO <sup>68</sup>	STD	384	9.48	0.49	0.07	0.1	0
	Mean	-924	1.81	0.39	0.19	0.15	0.04
BBO <sup>69</sup>	STD	65.7	1.05	0.57	0.11	0.45	0.06
	Mean	-989	4.83	2.15	0.48	0.41	0.31
BA <sup>70</sup>	STD	16.7	1.55	0.54	0.13	0.23	0.24
	Mean	-861	10.3	2.79	0.79	9.53	2220
BGSO <sup>71</sup>	STD	80.6	3.73	1.19	0.25	6.51	5660
	Mean	1	0.01	0.38	0.01	0.01	0.01
SCO <sup>72</sup>	STD	0.01	0.73	1	0.01	0.01	0.01
	Mean	0.06	0.01	0.2	0.01	0.14	0.08
SSO <sup>73</sup>	STD	0.81	0.01	0.15	0.07	0.56	0.71
	Mean	-8500	84.6	1.26	0.02	0.89	0.12
WOA <sup>74</sup>	STD	726	16.2	0.73	0.02	0.88	0.12
	Mean	-3140.3	1.63	0.73	0.02	0.88	0.19
BMFA1 <sup>75</sup>	STD	290.75	0.96	0.04	0	0	0
			0.96				
BMFA2 <sup>75</sup>	Mean	-3361.2		0	0	0	0 01
	STD	287.32	2.022602	0	0 002304	0 054082	0.01
E-GWO <sup>76,77</sup>	Mean	-5787.77	2.022602	0	0.002304	0.054082	0.655472
	STD	1251.334	3.476486	0	0.005280	0.030135	0.237728
hAGWOCS	Mean	-11,271.1	1.318777	0	0.006341	0.040212	0.627942
	STD	12,224.55	2.103797	0	0.012583	0.02329	0.235043

 Table 8. Comparison of multi-modal benchmark functions.

		Benchma	rk function	s			
Algorithms	Parameters	F14	F15	F16	F17	F18	F19
P0.054	Mean	3.63	0	-1.03	0.4	3	-3.86
PSO <sup>54</sup>	STD	2.56	0	0	0	0	0
00055	Mean	5.86	0	-1.03	0.4	3	-3.86
GSO <sup>55</sup>	STD	3.83	0	0	0	0	0
DE056	Mean	1	0	-1.03	0.4	3	NA
DEO <sup>56</sup>	STD	0	0	0	0	0	NA
PP-057	Mean	1.22	0	-0.03	0.4	3.02	-3.086
FFO <sup>57</sup>	STD	0.56	0	0	0	0.11	0
A.T. A.58	Mean	0	14.6	175	316	4.4	500
ALA <sup>58</sup>	STD	0	32.2	46.5	13	1.66	0.21
000059	Mean	776	873.8	961	899.86	741	900.5
SOSO <sup>59</sup>	STD	0	9.72	67.2	0	0.79	0.84
(0	Mean	182.48	487.2	588.2	756.98	542	818.5
BO <sup>60</sup>	STD	117.02	161.4	137.8	160.1	220	152.5
	Mean	0.34	18.23	224	362.03	10.2	504
FPO <sup>61,62</sup>	STD	0.24	3.07	50.3	54.02	1.39	1.16
	Mean	110	140.6	290	402	213	812
CS <sup>32</sup>	STD	110.05	92.8	86.1	92.2	206	192
	Mean	150.17	314.5	734	818.57	134	862
FO <sup>63</sup>	STD	97.16	92.93	204	204	216	126
	Mean	114.61	95.46	325.4	466.31	90.4	521.2
GO <sup>64</sup>	STD	26.96	7.16	51.67	29.57	13.7	27.99
	Mean	0	0.49	0	0.82	0	0.79
GOA <sup>65</sup>	STD	0.34	0.72	0	1	0.01	0.94
	Mean	2.11	0	-1.03	0.4	3	-3.86
MFO <sup>66</sup>	STD	1.5	0	0	0	0	0
	Mean	10	30.01	50	190.3	161	440
MVA <sup>67</sup>	STD	31.62	48.31	52.7	128.67	158	51.64
	Mean	104	193	458	596.66	230	680
DO <sup>68</sup>	STD	91.2	80.6	165	171.06	185	199
	Mean	1.39	1.02	10.5	1	1.01	1
BBO <sup>69</sup>	STD	1.19	10.7	1.49	1.11	1.01	1.2
	Mean	0.06	0	0.2	0	0.14	0.08
BA <sup>70</sup>	STD	0.81	0	0.15	0.07	0.56	0.71
	Mean	0	66.73	119	345.47	10.4	707
WOA <sup>74</sup>	STD	0	53.23	28.33	43.12	3.75	195
	Mean	12.61	0	-1.03	0	3	-3.86
BMFA1 <sup>75</sup>	STD	0.35	0	0	0	0	0
	Mean	12.61	0	-1.03	0	3	-3.86
BMFA2 <sup>75</sup>	STD	0.35	0	0	0	0	0
	Mean	3.714756	0.003812	-1.0.31628	0.397905	3.000042	-3.86165
E-GWO <sup>76,77</sup>	STD	3.486832	0.003812	0	0.397903	0.000068	0.002191
	Mean	4.581569	0.007333	-1.031628	0.397889	3.000049	-3.86271
hAGWOCS							
	STD	4.614445	0.000041	0	0.000002	0.000047	0.000100

**Table 9**. Comparison of fixed dimension benchmark functions.

level was kept at 10 cm for 300 to 400 s. The simulation results of the reference and the step responses of the QTS along with the control inputs are plotted in Figs. 11 and 12. The performances of the considered OH-FO-T2F-PID controller are compared with the performances of the optimized ADRC regulator and the OH-FO-T1F-PID regulator in terms of peak overshoot, peak time  $(t_p)$ , settling time  $(t_s)$ , and error (e). The obtained results are illustrated in Table 15. The Fig. 11 shows that the level control produced by the designed OH-FO-T2F-PID regulator has no overshoot and has a much lower settling time compared to optimized ADRC and OH-FO-T1F-PID. The closed-loop responses of QTS with OH-FO-T1F-PID regulator has overshoot, undershoot and long settling time, while the closed-loop responses of QTS with optimized ADRC regulator has less settling time and overshoot. There is a large difference between the control signals delivered to pumps 1 and 2 and what the considered OH-FO-T2F-PID and other controllers generate. The designed OH-FO-T2F-PID regulator provides

		Benchmark	functions		
Algorithms	Parameters	F20	F21	F22	F23
PSO <sup>54</sup>	Mean	-2.29	-7.89	-7.49	- 8.99
130	STD	1.06	3.07	4.08	1.76
GSO <sup>55</sup>	Mean	-2.36	- 4.99	-8.64	-10.63
GSO	STD	1.02	4.74	2.01	0
DEO <sup>56</sup>	Mean	0.01	-10.2	-10.4	-10.54
DEO	STD	0.01	0	0	0
FFO <sup>57</sup>	Mean	-4.28	-6.56	-6.57	-7.59
FFO	STD	0.08	1.57	2.18	3.18
WOA <sup>74</sup>	Mean	-2.98	-7.05	-8.18	-9.34
WOA	STD	0.38	3.63	3.83	2.41
BMFA1 <sup>75</sup>	Mean	-3.16	- 5.06	- 5.09	-5.13
DIVITAT	STD	0.08	0	0	0
BMFA2 <sup>75</sup>	Mean	-3.17	- 5.06	- 5.09	-5.013
DIVITAL	STD	0.12	0	0	0
E-GWO <sup>76,77</sup>	Mean	-3.264802	- 9.814392	- 9.969478	- 9.993865
E-GWO.	STD	0.075802	1.281744	1.670664	2.058353
hAGWOCS	Mean	-3.314051	-8.716156	-9.468602	-9.636681
IIAGWOCS	STD	0.030191	2.455752	2.134653	2.042330

Table 10. Comparison of fixed dimension benchmark functions.

approximately 5 Volt of flow rates to both motors with less aggressive control signals compared to the OH-FO-T1F-PID and optimized ADRC controller (Fig. 12). The aggressive effort from the OH-FO-T1F-PID regulator justifies the noticeable overflow in tank 1 and tank 2 levels. Conversely, by smoothly controlling the pump flows, the proposed OH-FO-T2F-PID regulator keeps tank levels from rising too high.

#### Test 2, tracking performance under sinusoidal set-point reference

In the second test, a reference signal consisting of a 3 cm sine wave with a bias of 10 cm and a period of 60 s was utilized to track the change in the liquid level inside the tank. The simulation responses of the tank liquid level and control inputs are depicted in Figs. 13 and 14. As the results show, the designed OH-FO-T2F-PID regulator provided accurate level control performance with rapid settling and without overshoot. Compared with the OH-FO-T1F-PID regulator and optimized ADRC regulator, the suggested OH-FO-T2F-PID regulator provided better reference tracking dynamics.

#### Test 3, tracking performance under external perturbations

To evaluate the tracking performance of the designed OH-FO-T2F-PID regulator against external perturbations, the following test was conducted: The liquid level h2 increases to 7 cm. Next, it rises by 3 cm at the time instant t=100 s to arrive at 10 cm. At the moment t=200 s, a perturbation occurs as a step signal with changeable amplitude (1 cm from t=200 s to t=300 s, and -2 cm for the remaining time of the test), which is practically explained by adding an amount of liquid and opening the discharge valve to produce a little leak within the tank. The simulation outcomes of the evolution of the tank liquid level and the control inputs are illustrated in Figs. 15 and 16.

#### Test 4, tracking performance under parameter uncertainty

This test analyzes the influence of parameter uncertainty on the QTS. One of the parameters that affects the performance of the QTS is uncertainty in the design of the outlet hole of the first tank. Figures 17 and 18 illustrate the output response and the control inputs of the first tank, respectively, in the presence of parameter uncertainty ( $\Delta k_1 = -50\%$ ) after 200 s of the test beginning. As presented in Figs. 17 and 18, the designed OH-FO-T2F-PID regulator shows superior ability to smoothly manage parameter fluctuations. In contrast, the optimized ADRC regulator shows a deviation of –10.17% from the steady state. While, the OH-FO-T1F-PID regulator requires about 30 s to mitigate the influence of uncertainty. On the other hand, the suggested OH-FO-T2F-PID regulator effectively reduces the influence of parameter changes, highlighting its robustness and improved response.

#### **HIL** experiment validation

In this section, real-time HIL-based experiments are performed using the following hardware setup (Fig. 19). Where the external threads comprise the hardware components interfaced with the software for real-time control and feedback. These include critical elements such as the Data Acquisition System (DAQ), and real-time controller (dSPACE), which executes the control algorithm (OH-FO-T2F-PID regulator) and ensures deterministic communication with the host PC. Whereas, the internal threads encompass the software components running on the real-time simulation platform. These threads integrate a high-fidelity mathematical model of the QTS, developed in MATLAB/Simulink. Additionally, it incorporate ControlDesk monitoring tools, such as interactive

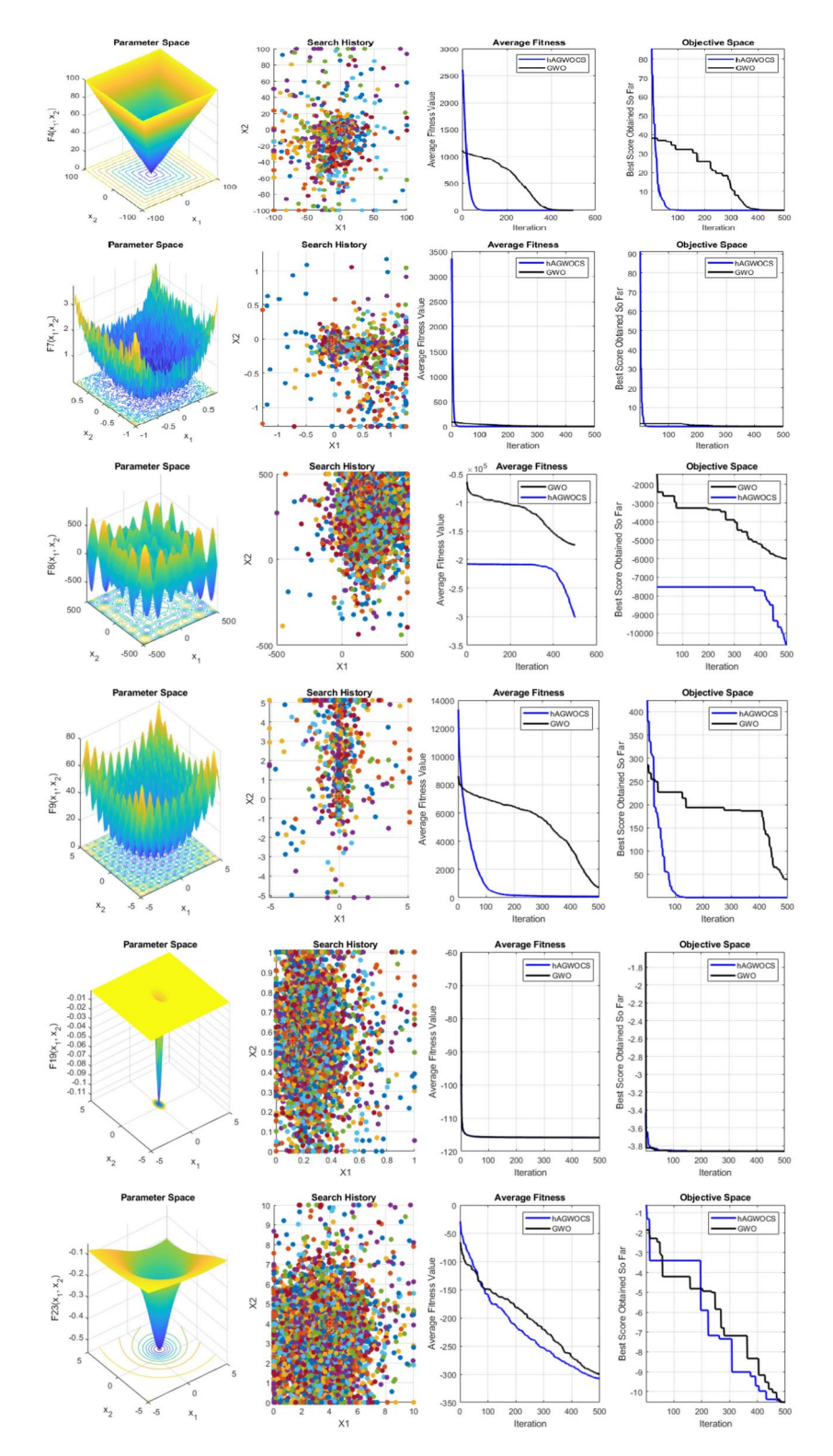


Fig. 8. Results of qualitative analysis by hAGWOCS and regular GWO methods.

dashboards and data visualization interfaces, to track QTS performance metrics (tracking errors) and verify the effectiveness of the suggested OH-FO-T2F-PID regulator. Together, these threads seamlessly interact to simulate real-world QTS behavior while enabling rigorous testing of control robustness under external disturbances and parameter uncertainties. The prototype device, which was utilized to demonstrate the robustness and reliability of the designed OH-FO-T2F-PID regulator is illustrated in Fig. 19a. The system's hardware comprises a host PC, a numerical oscilloscope, and a dSPACE-ds1104 digital controller. The latter is a real-time simulator based on a fully digital signal processor responsible for converting and generating the control. Whereas the QTS, and

Regulator coefficients	$G_{E}$	$G_{DE}$	$G_{PD}$	$G_{PI}$	λ	μ
Lower bound (min)	0.001	0.001	0.001	0.001	0.1	0.1
Upper bound (max)	10	10	10	10	2	2

Table 11. Bounds of the gains of the FO-T2F-PID regulator hAGWOCS method.

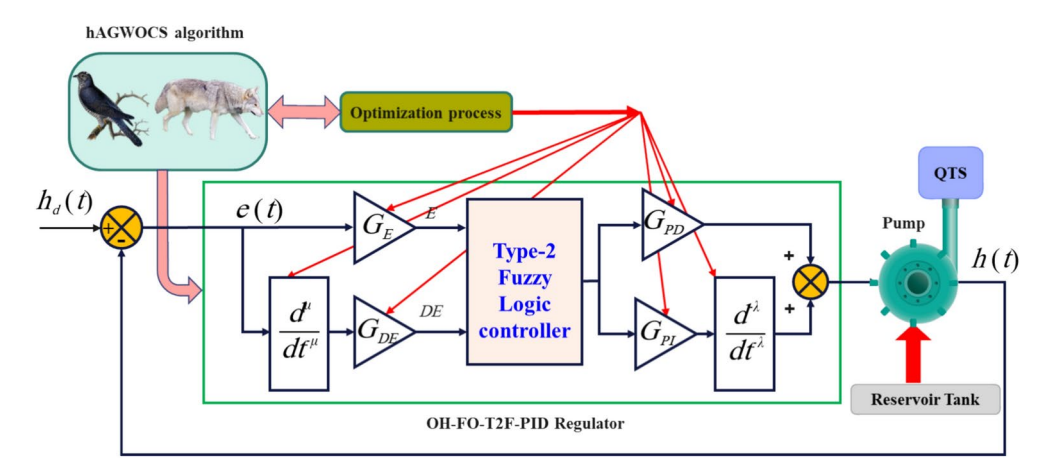


Fig. 9. Schematic diagram of the optimization process of OH-FO-T2F-PID regulator.

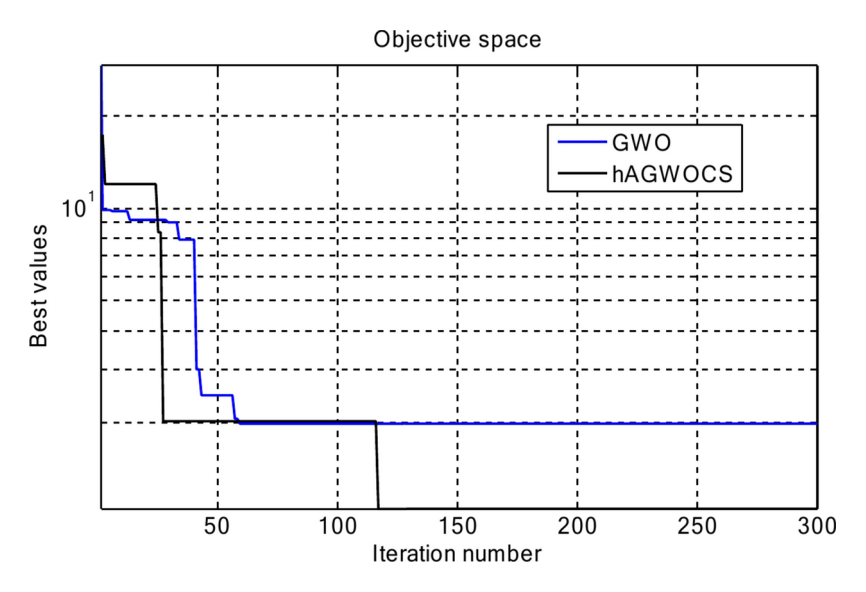


Fig. 10. Convergence profiles of GWO and hAGWOCS methods using OH-FO-T2F-PID regulator after 50 trials.

Parameters	Value	Parameters	Value	
$G_E$	0.91	$G_{PI}$	3.85	
$G_{DE}$	0.85	λ	0.95	
$G_{PD}$	0.63	μ	0.93	

Table 12. Optimal design for OH-FO-T2F-PID regulator gains by hAGWOCS algorithm.

Parameters	Value	Parameters	Value	
$G_E$	0.89	$G_{PI}$	4.15	
$G_{DE}$	0.81	λ	0.92	
$G_{PD}$	0.74	μ	0.94	

Table 13. Optimal design OH-FO-T1F-PID regulator gains by hAGWOCS algorithm.

Parameters	Value	Parameters	Value	
$\alpha_1$	0.57	$\alpha_2$	0.21	
$\delta_1$	0.013	$\delta_2$	1.91	
$\omega_{01}$	145.23	$\omega_{02}$	168.11	
$b_{01}$	1.20	$b_{02}$	1.02	

Table 14. Optimal design for ADRC regulator gains by hAGWOCS algorithm.

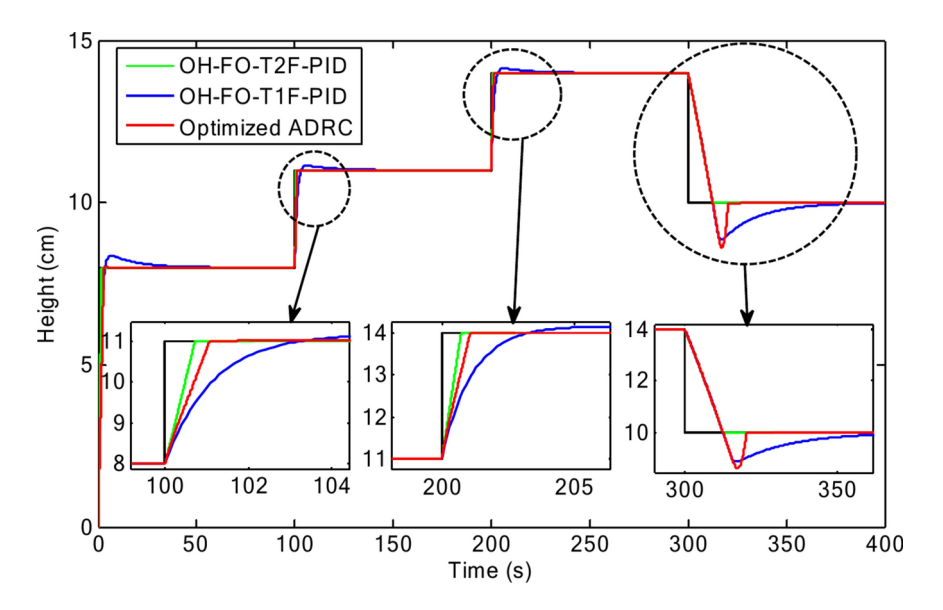


**Fig. 11**. Liquid level evolution for step-point tracking test.

liquid level sensors are simulated using the MATLAB/Simulink, following the schematic diagram of Fig. 19b. The performance of the designed OH-FO-T2F-PID controller was validated by conducting two practical tests on QTS.

#### Test 1, reference tracking control

Figure 20 displays the first experimental output responses of the reference tracking control when the objective is to follow two successive step trajectories for water levels  $h_1$  and  $h_2$ , respectively. The control test duration is 100 s. It is necessary to announce that the state trajectories have been selected in such a way that large variations in different equilibrium points are included. These variations were applied at two times throughout the experiment at  $t_1$  = 10 s and  $t_2$  = 50 s. The maximum tank levels ( $h_{max}$ ) are 14 cm. The proposed OH-FO-T2F-PID regulator has been tested and the findings are illustrated in Fig. 20. According to Fig. 20, the designed OH-FO-T2F-PID regulator exhibits excellent tracking performances because the output trajectories follow their references without overshoot, and the steady-state tracking error is greatly reduced to a small neighbourhood of zero. It is worth noticing that the experimental results very are close to the simulation results.

#### Test 2, external disturbance rejection

The designed OH-FO-T2F-PID regulator can also be utilized to solve the disturbance rejection problem. Figure 21 displays the practical outcomes of the recommended OH-FO-T2F-PID controller against external disturbance rejection issue. In this test, the disturbance is applied at the 80th second, by pouring more water into tank 1, causing an increase in the  $h_1$  level of about 10%–20% as shown in Fig. 21. The designed OH-FO-T2F-PID regulator showed good properties in closed-loop experiments, and also showed stable and viable trajectories even in the existence of perturbations. It is necessary to emphasize that in the second experiment, the suggested OH-FO-T2F-PID regulator decreases the control signal to allow tank 1 to leak until the desired response (Fig. 22). As

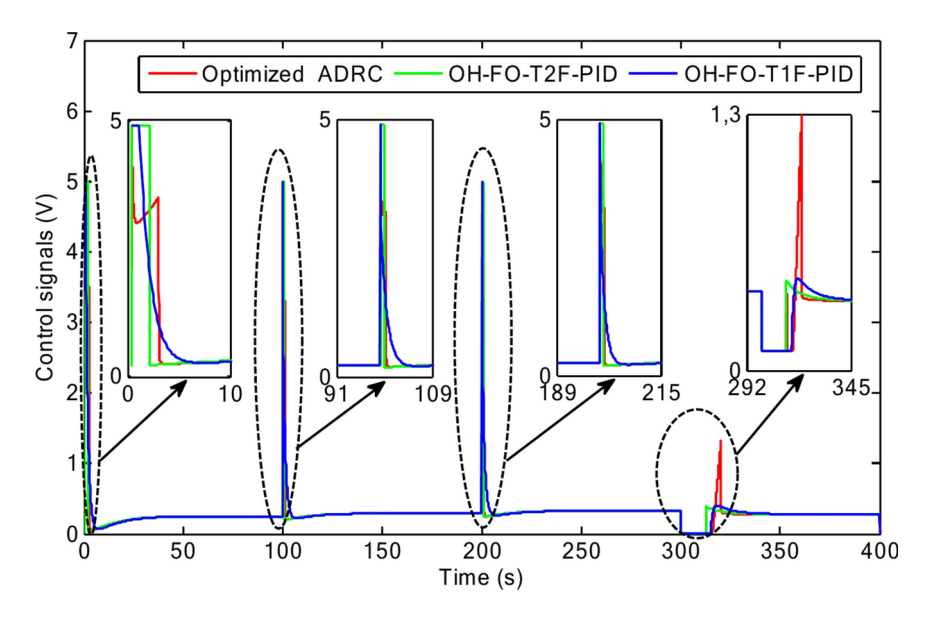


Fig. 12. Control inputs evolution for step-point tracking test.

Switching instant	Regulator	Overshoot (%)	$t_p(s)$	$t_s(s)$	e (%)
0 s (0-7 cm)	OH-FO-T2F-PID	_	-	2.4	0.0002
	OH-FO-T1F-PID	4.37	6.4	44.5	0.025
	Optimized ADRC <sup>78</sup>	0.08	4.14	7.2	0.1
100 s (7–11 cm)	OH-FO-T2F-PID	-	-	0.8	0.004
	OH-FO-T1F-PID	1.28	5.5	40.7	0.09
	Optimized ADRC <sup>78</sup>	0.50	1.8	8.1	0.12
200 s (11–14 cm)	OH-FO-T2F-PID	-	-	0.8	0.005
	OH-FO-T1F-PID	1.02	5.9	40.2	0.04
	Optimized ADRC <sup>78</sup>	0.35	2.7	4.7	0.7
300 s (14–11 cm)	OH-FO-T2F-PID	_	-	12.5	0.004
	OH-FO-T1F-PID	-11.45	17	77.1	2
	Optimized ADRC <sup>78</sup>	-13.96	17.2	20.8	0.17

**Table 15**. Dynamic behavior of the three studied regulators.

shown in Fig. 21, the high quality of the tracking response is not affected by the injected disturbance. Therefore, the recommended control strategy is also effective in rejecting small external disturbances.

#### **HIL Experiment limitations**

A number of difficulties arise while testing and implementing the suggested OH-FO-T2F-PID regulator in real-time HIL system due to its intrinsic complexity. The following are the main limitations of using the OH-FO-T2F-PID regulator in a HIL experiment:

- The OH-FO-T2F-PID regulator includes a fractional-degree and a type-2 fuzzy logic system, which are computationally intensive and difficult to implement in real-time HIL simulation.
- Tuning the parameters of the suggested OH-FO-T2F-PID regulator is a complex and time-consuming process.
- The mismatch between the simulation model and the physical hardware can lead to inaccurate results.
- The final challenge of the HIL Experiment is to deal with practical issues such as computation delays, communication failures, and software errors. These issues can affect data quality, the feasibility, and the reliability of the HIL experiment.

#### Conclusion and future scope

In this study, the Fuzzy type-2 system is combined with the fractional calculus to design a robust OH-FO-T2F-PID regulator for precise liquid level tracking in a state-coupled QTS. The hybrid GWO-CS algorithm was utilized to choose the optimal gains for the recommended OH-FO-T2F-PID regulator. The improvements were made by incorporating the efficient exploitation mechanism of the A-GWO method with exploration

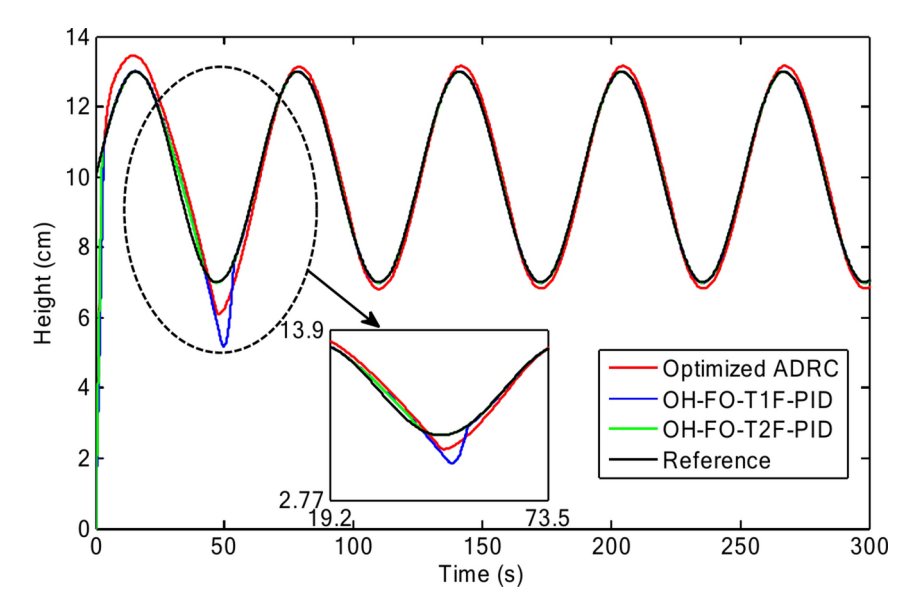


Fig. 13. Liquid level evolution for sinusoidal set-point tracking test.

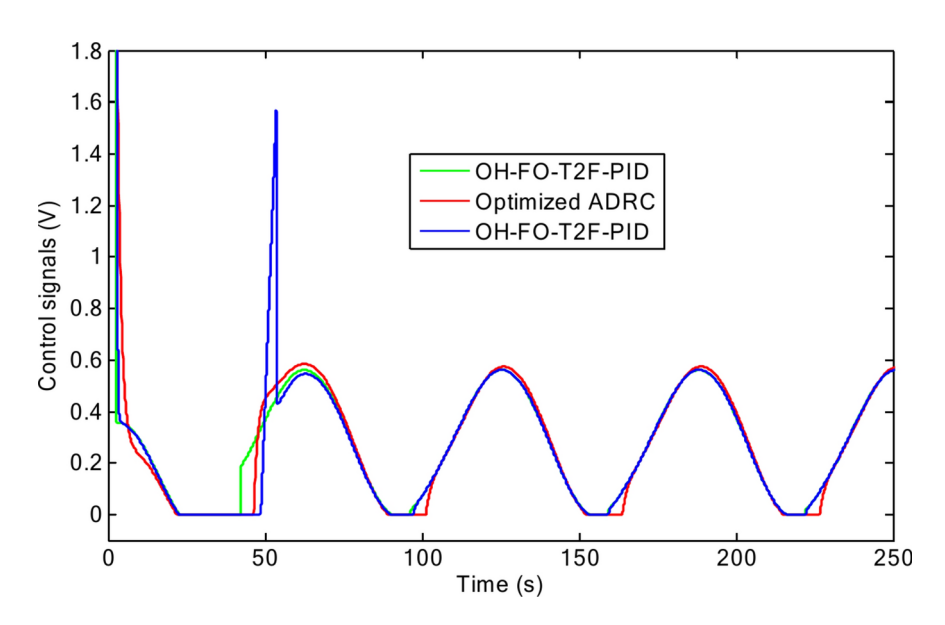


Fig. 14. Control signals evolution for sinusoidal set-point test.

capabilities of the CS method. The suggested hybrid A-GWOCSO method has been tested to select the best coefficients of the OH-FO-T2F-PID regulator. To validate the control performance, simulations and real-time control experiments were conducted using the HIL test bench on QTS, and the control results of the optimized ADRC and OH-FO-T1F-PID regulators, along with the suggested OH-FO-T2F-PID regulator, were presented to establish a comprehensive comparison. The findings of the simulation and HIL testing demonstrated that the suggested OH-FO-T2F-PID regulator outperformed the optimized ADRC and the OH-FO-T1F-PID regulators in terms of references tracking, parameters uncertainty, and external perturbations elimination. A statistical comparison of the suggested Hybrid A-GWOCSO method with 23 recently reported optimizer is also carried out with 30 independent runs. It is found that the hAGWOCS method outperforms thirteen compared methods in terms of accuracy, and is only worse than ten compared methods.

Although the suggested OH-FO-T2F-PID regulator displays significant improvement in QTS performance compared to its counterparts, it should also be noted that the OH-FO-T2F-PID regulator is more complex and requires more computations. Therefore, it may not be suitable for all applications, particularly those where simplicity is important or where computational resources are limited.

As a next research, the new IT2FO-FPID regulator should be investigated for practical problems that are more susceptible to parameter fluctuations, disturbances, and random noise. The stability analyses of the suggested IT2FO-FPID regulator should also be studied to improve its robustness. We hope that the recommended multi-

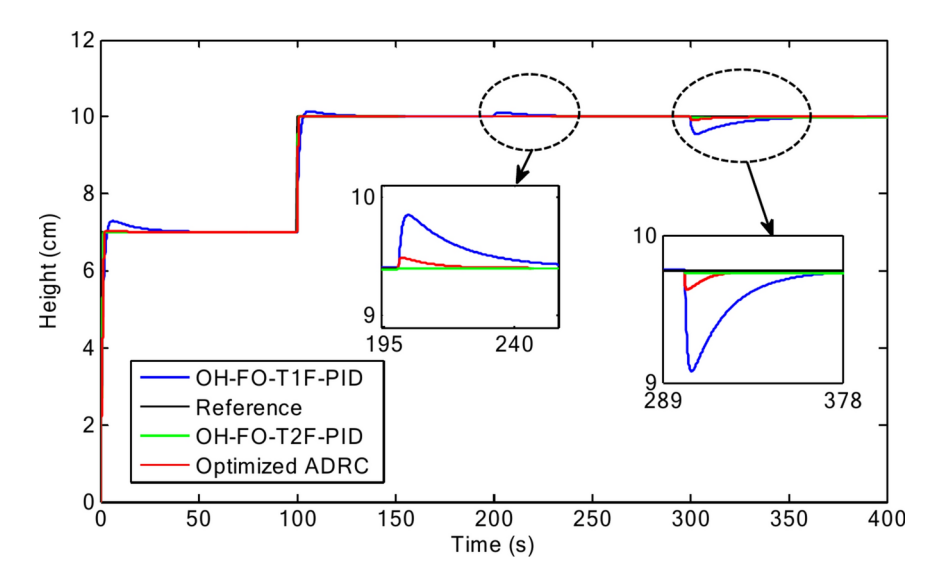


Fig. 15. Liquid level evolution for external disturbance test.

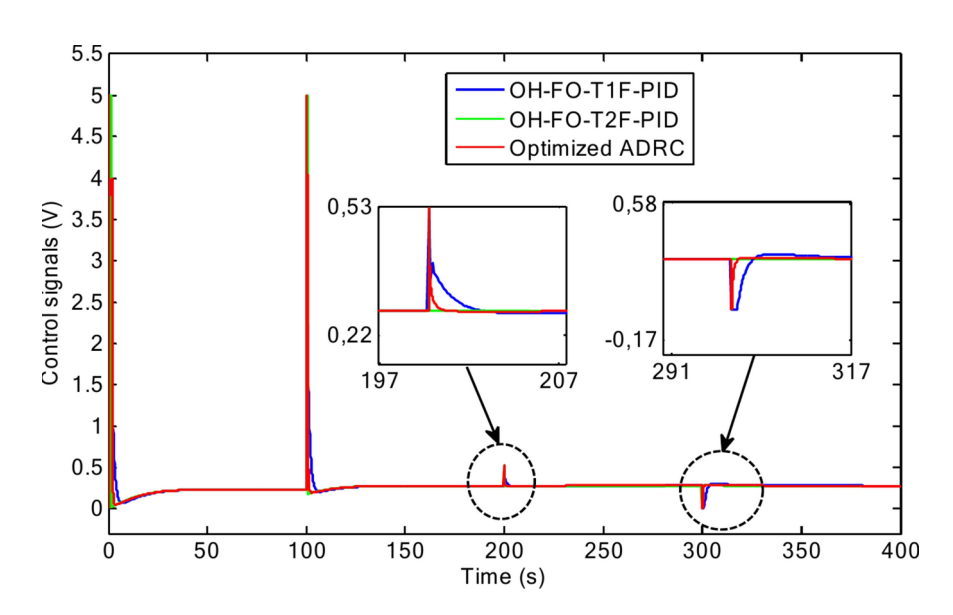


Fig. 16. Control signals evolution for external disturbance test.

objective optimization strategy will be useful in adjusting the gains of the OH-IT2FO-FPID regulator and will provide successful results in the future.

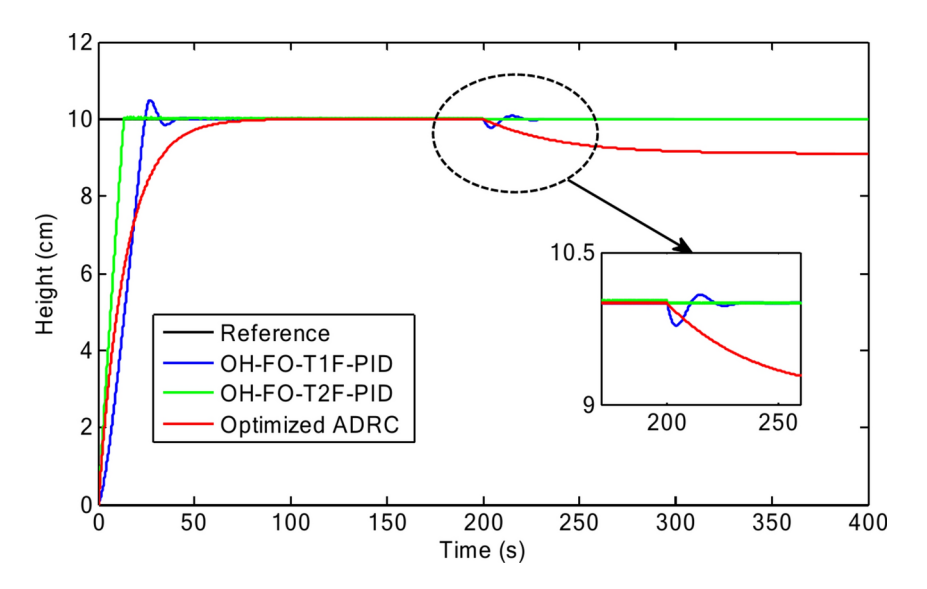


Fig. 17. Liquid level evolution with uncertainty in the outlet hole of tank1.

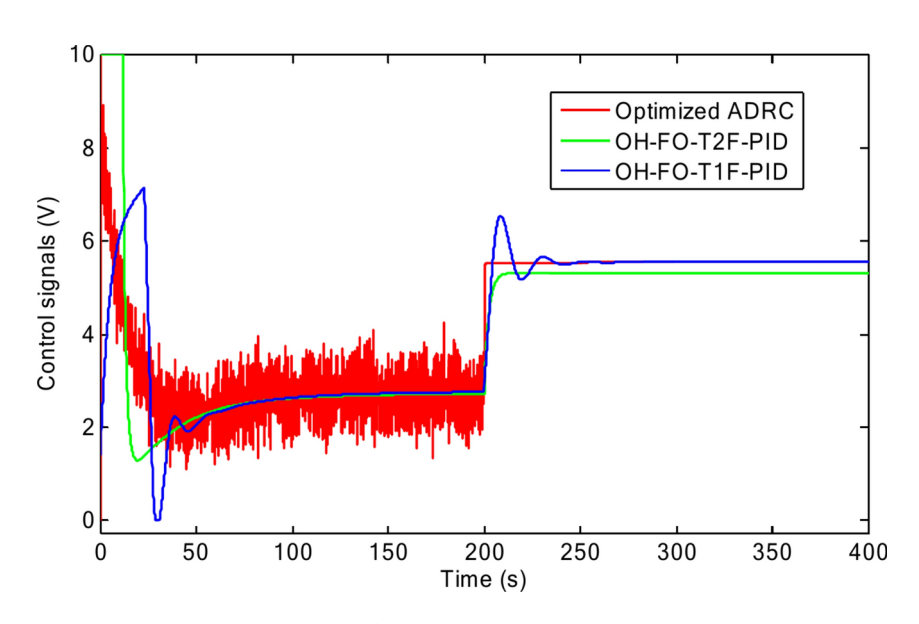


Fig. 18. Control signals evolution for parameter uncertainty test.

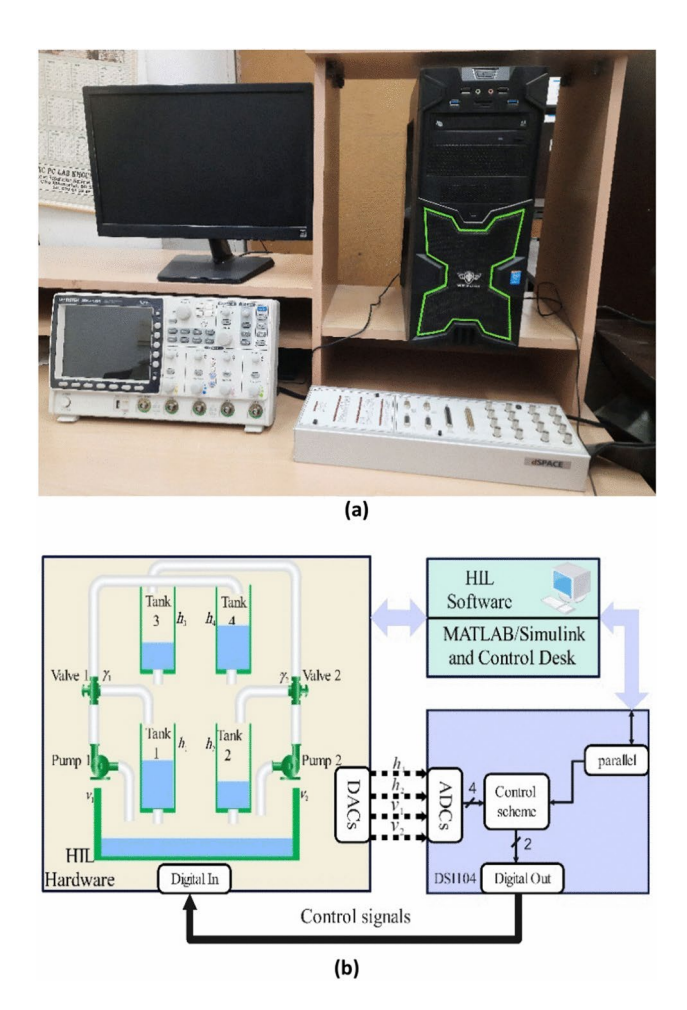


Fig. 19. The hardware implementation (a), and the Flowchart for HIL-based laboratory testing setup (b).

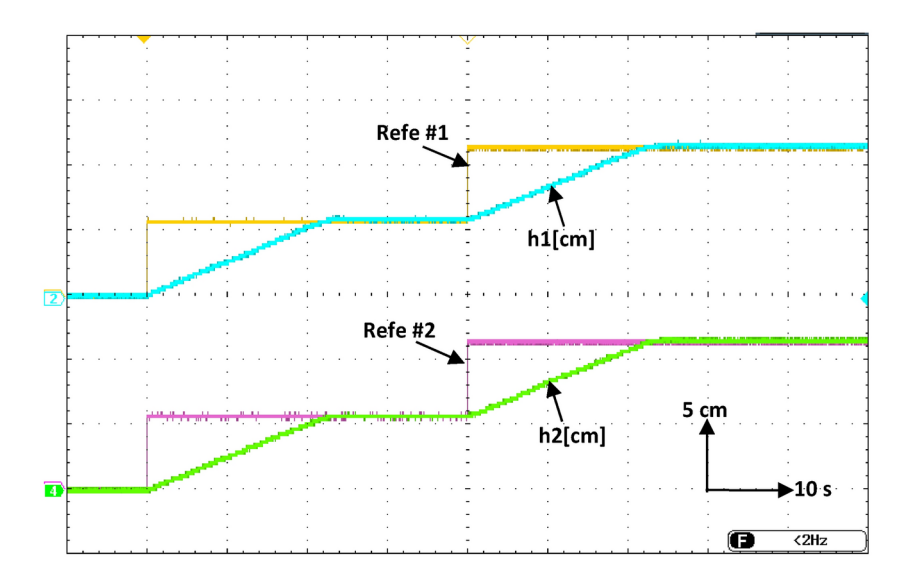


Fig. 20. Practical results of the designed OH-FO-T2F-PID regulator for reference tracking test.

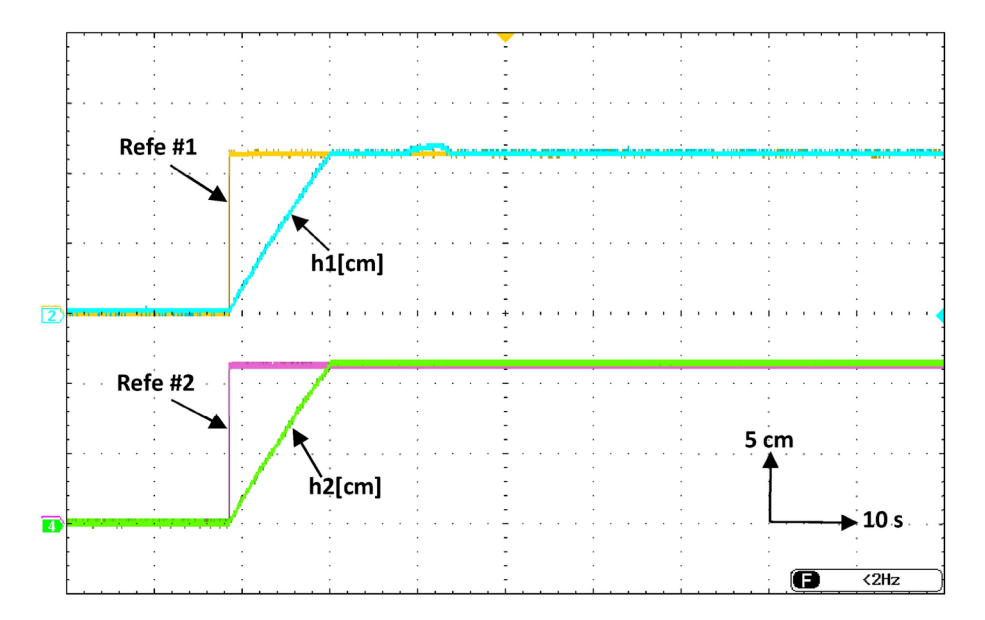


Fig. 21. Practical results of the designed OH-FO-T2F-PID regulator for external disturbance rejection test.

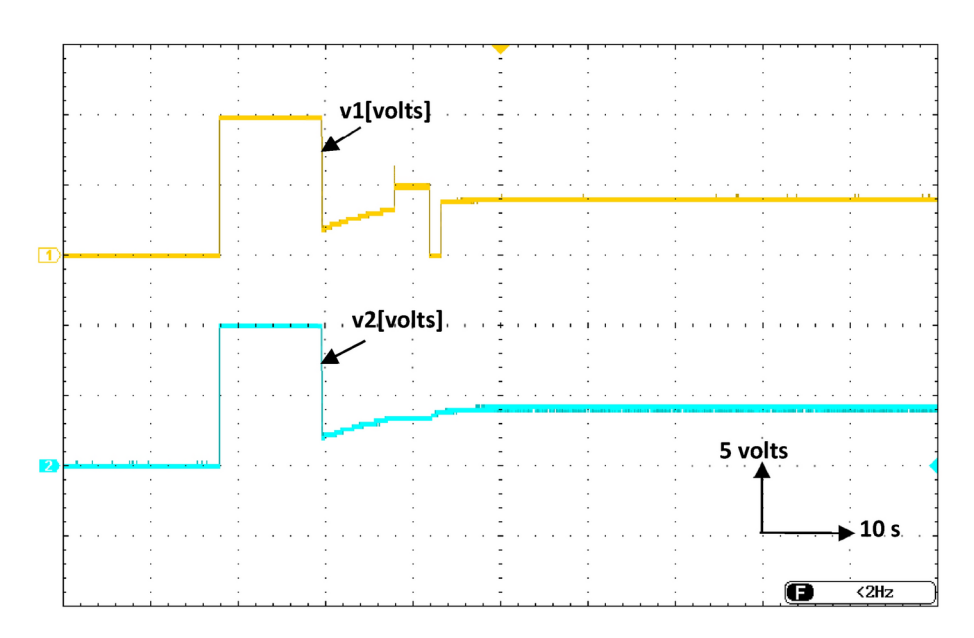


Fig. 22. Practical response of control input of both the tanks during external disturbance.

#### Data availability

The datasets used and/or analyzed during the current study available from the corresponding author on reasonable request.

Received: 14 November 2024; Accepted: 24 February 2025 Published online: 04 March 2025

#### References

- 1. Mahapatro, S. R., Subudhi, B. & Ghosh, S. Design and experimental realization of a robust decentralized PI controller for a coupled tank system. *ISA Trans.* 89, 158–168. https://doi.org/10.1016/j.isatra.2018.12.003 (2019).
- Chekari, T., Mansouri, R. & Bettayeb, M. Real-time application of IMC-PID-FO multi-loop controllers on the coupled tanks process. Proc. Inst. Mech. Eng. I J. Syst. Control Eng. 235, 1542–1552. https://doi.org/10.1177/0959651820983062 (2021).
- 3. Holič, I. & Veselý, V. Robust PID controller design for coupled-tank process using Labreg software. IFAC Proc. Vol. 45, 442–447. https://doi.org/10.3182/20120619-3-ru-2024.00100 (2012).
- 4. Son, N. N. Level control of quadruple tank system based on adaptive inverse evolutionary neural controller. *J. Control Autom. Syst.* **18**, 2386–2397. https://doi.org/10.1007/s12555-019-0504-8 (2020).

- Meng, X., Yu, H., Wu, H. & Xu, T. Disturbance observer-based integral backstepping control for a two-tank liquid level system subject to external disturbances. Math. Probl. Eng. 2020, 1–22. https://doi.org/10.1155/2020/6801205 (2020).
- Chaudhari, V., Tamhane, B. & Kurode, S. Robust liquid level control of quadruple tank system-second order sliding mode approach. IFAC Pap. Online 53, 7–12. https://doi.org/10.1016/j.ifacol.2020.06.002 (2020).
- 7. Meng, X., Yu, H., Zhang, J., Xu, T. & Wu, H. Liquid level control of four-tank system based on active disturbance rejection technology. *Measurement* 175, 109146. https://doi.org/10.1016/j.measurement.2021.109146 (2021).
- 8. Thamallah, A., Sakly, A. & M'Sahli, F. A new constrained PSO for fuzzy predictive control of quadruple-tank process. *Measurement* 136, 93–104. https://doi.org/10.1016/j.measurement.2018.12.050 (2019).
- 9. Xu, J., Li, C., He, X. & Huang, T. Recurrent neural network for solving model predictive control problem in application of four-tank benchmark. *Neurocomputing* 190, 172–178. https://doi.org/10.1016/j.neucom.2016.01.020 (2016).
- Johansson, K. H. The quadruple-tank process: A multivariable laboratory process with an adjustable zero. IEEE Trans. Control Syst. Technol. 8, 456–465. https://doi.org/10.1109/87.845876 (2000).
- Vo, L. C., Nguyen, L. V. T. & Lee, M. Fractional order modeling and control of a quadruple-tank process. In 2020 5th International Conference on Green Technology and Sustainable Development (GTSD) 334–339 (2020). https://doi.org/10.1109/gtsd50082.2020.9 303059
- 12. Gheisarnejad, M. An effective hybrid harmony search and cuckoo optimization algorithm based fuzzy PID controller for load frequency control. *Appl. Soft Comput.* **65**, 121–138. https://doi.org/10.1016/j.asoc.2018.01.007 (2018).
- 13. Zadeh, L. A. The concept of a linguistic variable and its application to approximate reasoning—I. *Inf. Sci.* 8, 199–249. https://doi.org/10.1016/0020-0255(75)90036-5 (1975).
- 14. Fayek, H. M., Elamvazuthi, I., Perumal, N. & Venkatesh, B. A controller based on optimal type-2 fuzzy logic: Systematic design, optimization and real-time implementation. *ISA Trans.* 53, 1583–1591. https://doi.org/10.1016/j.isatra.2014.06.001 (2014).
- 15. Cao, J., Li, P. & Liu, H. An interval fuzzy controller for vehicle active suspension systems. *IEEE Trans. Intell. Transp. Syst.* 11, 885–895. https://doi.org/10.1109/tits.2010.2053358 (2010).
- Kumar, A. & Kumar, V. Design of interval type-2 fractional-order fuzzy logic controller for redundant robot with artificial bee colony. Arab. J. Sci. Eng. 44, 1883–1902. https://doi.org/10.1007/s13369-018-3207-1 (2018).
- 17. Kuttomparambil Abdulkhader, H., Jacob, J. & Mathew, A. T. Robust type-2 fuzzy fractional order PID controller for dynamic stability enhancement of power system having RES based microgrid penetration. *Int. J. Electr. Power Energy Syst.* 110, 357–371. https://doi.org/10.1016/j.ijepes.2019.03.027 (2019).
- 18. Cervantes, L. & Castillo, O. Type-2 fuzzy logic aggregation of multiple fuzzy controllers for airplane flight control. *Inf. Sci.* 324, 247–256. https://doi.org/10.1016/j.ins.2015.06.047 (2015).
- 19. Anbalagan, P. & Joo, Y. H. Stabilization analysis of fractional-order nonlinear permanent magnet synchronous motor model via interval type-2 fuzzy memory-based fault-tolerant control scheme. *ISA Trans.* 142, 310–324. https://doi.org/10.1016/j.isatra.2023. 08.021 (2023).
- 20. Sahu, P. C., Baliarsingh, R., Prusty, R. C. & Panda, S. Automatic generation control of diverse energy source-based multiarea power system under deep Q-network-based fuzzy-T2 controller. *Energy Sources A Recov. Util. Environ. Eff.* 46, 15125–15146 (2020).
- Chhabra, H., Mohan, V., Rani, A. & Singh, V. Robust nonlinear fractional order fuzzy PD plus fuzzy I controller applied to robotic manipulator. Neural Comput. Appl. 32, 2055–2079. https://doi.org/10.1007/s00521-019-04074-3 (2019).
- Ranjan, M., Shankar, R., Saxena, A. & Rai, P. Design and analysis of novel QOAOA optimized Type-2 fuzzy FOPIDN controller for AGC of multi-area power system. In 2022 2nd International Conference on Emerging Frontiers in Electrical and Electronic Technologies (ICEFEET) 1-6 (2022). https://doi.org/10.1109/icefeet51821.2022.9847973.
- 23. Sikander, A., Thakur, P., Bansal, R. C. & Rajasekar, S. A novel technique to design cuckoo search based FOPID controller for AVR in power systems. *Comput. Electr. Eng.* 70, 261–274. https://doi.org/10.1016/j.compeleceng.2017.07.005 (2018).
- Zamani, A.-A. & Etedali, S. Seismic structural control using magneto-rheological dampers: A decentralized interval type-2 fractional-order fuzzy PID controller optimized based on energy concepts. ISA Trans. 137, 288–302. https://doi.org/10.1016/j.isat ra.2023.02.001 (2023).
- 25. Mohammadikia, R. & Aliasghary, M. Design of an interval type-2 fractional order fuzzy controller for a tractor active suspension system. *Comput. Electron. Agric.* 167, 105049. https://doi.org/10.1016/j.compag.2019.105049 (2019).
- Xu, Y. et al. Design of type-2 fuzzy fractional-order proportional-integral-derivative controller and multi-objective parameter optimization under load reduction condition of the pumped storage unit. J. Energy Storage 50, 104227. https://doi.org/10.1016/j.e st.2022.104227 (2022).
- 27. Oussama, M., Abdelghani, C. & Lakhdar, C. Efficiency and robustness of type-2 fractional fuzzy PID design using salps swarm algorithm for a wind turbine control under uncertainty. ISA Trans. 125, 72–84. https://doi.org/10.1016/j.isatra.2021.06.016 (2022).
- 28. Kumar, A. & Kumar, V. A novel interval type-2 fractional order fuzzy PID controller: Design, performance evaluation, and its optimal time domain tuning. *ISA Trans.* **68**, 251–275. https://doi.org/10.1016/j.isatra.2017.03.022 (2017).
- 29. Zhao, W. et al. Electric eel foraging optimization: A new bio-inspired optimizer for engineering applications. *Expert Syst. Appl.* 238, 122200. https://doi.org/10.1016/j.eswa.2023.122200 (2024).
- 30. Kahla, S., Boutaghane, A., Abdallah, L. et al. Grey wolf optimization of fractional PID controller in gas metal arc welding process. In the 5th International Conference on Control Engineering and Information Technology (CEIT-2017), Sousse-Tunisia (2017).
- 31. Babes, B., Albalawi, F., Hamouda, N., Kahla, S. & Ghoneim, S. S. M. Fractional-fuzzy PID control approach of photovoltaic-wire feeder system (PV-WFS): simulation and HIL-based experimental investigation. *IEEE Access* 9, 159933–159954. https://doi.org/10.1109/access.2021.3129608 (2021).
- 32. Yang, X.-S. & Deb, S. Cuckoo search: Recent advances and applications. *Neural Comput. Appl.* 24, 169–174. https://doi.org/10.1007/s00521-013-1367-1 (2013).
- 33. Hamouda, N. et al. Optimal tuning of fractional order proportional-integral-derivative controller for wire feeder system using ant colony optimization. *J. Européen des Systèmes Automatisés* 53, 157–166. https://doi.org/10.18280/jesa.530201 (2020).
- Hamouda, N., Babes, B., Boutaghane, A. & Hamouda, C. A robust PI<sup>λ</sup>D<sup>μ</sup> controller for enhancing the width of the molten pool and the tracking of welding current in gas metal arc welding (GMAW) processes. *Int. J. Model. Simul.* https://doi.org/10.1080/0228620 3.2023.2243061 (2023).
- 35. Bhatta, S. K. et al. Load frequency control of a diverse energy source integrated hybrid power system with a novel hybridized harmony search-random search algorithm designed Fuzzy-3D controller. *Energy Sources A Recov. Util. Environ. Eff.* **66**, 1–22 (2021).
- 36. Sahu, P. C. & Samantaray, S. R. Resilient frequency stability of a PV/wind penetrated complex power system with CSA tuned robust type-2 fuzzy cascade PIF controller. *Electr. Power Syst. Res.* **225**, 109815 (2023).
- 37. Jabari, M. et al. Efficient DC motor speed control using a novel multi-stage FOPD(1 + PI) controller optimized by the Pelican optimization algorithm. Sci. Rep. 14, 66 (2024).
- 38. Jabari, M. et al. Performance analysis of DC–DC Buck converter with innovative multi-stage PIDn(1+PD) controller using GEO algorithm. Sci. Rep. 14, 66 (2024).
- 39. Alzakari, S. A. et al. Nonlinear FOPID controller design for pressure regulation of steam condenser via improved metaheuristic algorithm. *PLoS ONE* **19**, e0309211 (2024).
- Ekinci, S., Izci, D., Turkeri, C. & Ahmad, M. A. Spider wasp optimizer-optimized cascaded fractional-order controller for load frequency control in a photovoltaic-integrated two-area system. *Mathematics* 12, 3076 (2024).

- 41. Eker, E. et al. Efficient voltage regulation: An RW-ARO optimized cascaded controller approach. e-Prime Adv. Electr. Eng. Electron. Energy 9, 100687 (2024).
- Long, W., Cai, S., Jiao, J., Xu, M. & Wu, T. A new hybrid algorithm based on grey wolf optimizer and cuckoo search for parameter extraction of solar photovoltaic models. Energy Convers. Manag. 203, 112243. https://doi.org/10.1016/j.enconman.2019.112243
- 43. Bouaddi, A., Rabeh, R. &Ferfra, M. Load frequency control of autonomous microgrid system using hybrid fuzzy logic GWO-CS PI controller. In 2021 9th International Conference on Systems and Control (ICSC) 554-559 (2021). https://doi.org/10.1109/icsc50 472.2021.9666683.
- 44. Long, W., Cai, S., Jiao, J., Xu, M. & Wu, T. A new hybrid algorithm based on grey wolf optimizer and cuckoo search for parameter extraction of solar photovoltaic models. Energy Convers. Manag. https://doi.org/10.1016/j.enconman.2019.112243 (2020).
- 45. Sahu, P. C., Prusty, R. C. & Panda, S. Improved-GWO designed FO based type-II fuzzy controller for frequency awareness of an AC microgrid under plug in electric vehicle. J. Ambient Intell. Hum. Comput. 12, 1879-1896. https://doi.org/10.1007/s12652-020-022 60-z (2020).
- 46. Kumar, A. & Kumar, V. Performance analysis of optimal hybrid novel interval type-2 fractional order fuzzy logic controllers for fractional order systems. Expert Syst. Appl. 93, 435-455. https://doi.org/10.1016/j.eswa.2017.10.033 (2018).
- 47. Mirjalili, S., Mirjalili, S. M. & Lewis, A. Grey wolf optimizer. Adv. Eng. Softw. 69, 46-61. https://doi.org/10.1016/j.advengsoft.2013 .12.007 (2014).
- 48. Qais, M. H., Hasanien, H. M. & Alghuwainem, S. Augmented grey wolf optimizer for grid-connected PMSG-based wind energy conversion systems. Appl. Soft Comput. 69, 504-515. https://doi.org/10.1016/j.asoc.2018.05.006 (2018).
- Yang, X.-S. & Deb, S. Cuckoo search via Lévy flights. In 2009 World Congress on Nature & Biologically Inspired Computing (NaBIC). https://doi.org/10.1109/nabic.2009.5393690.
- 50. Yang, X.-S. Nature-Inspired Optimization Algorithms (Academic Press, 2020).
- 51. Long, W., Cai, S., Jiao, J., Xu, M. & Wu, T. A new hybrid algorithm based on grey wolf optimizer and cuckoo search for parameter extraction of solar photovoltaic models. Energy Convers. Manag. 203, 112243. https://doi.org/10.1016/j.enconman.2019.112243
- 52. Yang, X.-S. & Deb, S. Cuckoo search via Lévy flights. In 2009 World Congress on Nature & Biologically Inspired Computing (NaBIC). https://doi.org/10.1109/nabic.2009.5393690.
- Nakayama, K., Fujita, G. & Yokoyama, R. Load frequency control for utility interaction of wide-area power system interconnection. In Transmission & Distribution Conference & Exposition: Asia and Pacific 1-4 (2009).
- 54. Kahla, S. et al. Maximum power extraction framework using robust fractional-order feedback linearization control and GM-CPSO for PMSG-based WECS. Wind Eng. 45, 1040-1054 (2020).
- 55. Rashedi, E., Nezamabadi-Pour, H. & Saryazdi, S. G. S. A. A gravitational search algorithm. Inf. Sci 179, 2232-2248 (2009).
- Panda, G., Sidhartha, P. & Cemal, A. Automatic generation control of interconnected power system with generation rate constraints by hybrid neuro fuzzy approach. World Acad. Sci. Eng. Technol. 52, 543-548 (2009).
- 57. Mirjalili, S. et al. Salp swarm algorithm: A bio-inspired optimizer for engineering design problems. Adv. Eng. Softw 114, 163–191 (2017).
- 58. Tan, Y., Tan, Y. & Zhu, Y. Fireworks algorithm for optimization fireworks algorithm for optimization. IEEE Trans. 1, 355-364 (2015).
- 59. Li, M. D., Zhao, H., Weng, X. W. & Han, T. A novel nature-inspired algorithm for optimization: Virus colony search. Adv. Eng. Softw. 92, 65-88 (2016).
- Yang, X.-S. A new metaheuristic bat-inspired algorithm. In Nature Inspired Cooperative Strategies for Optimization vol. 1 65-74 (Springer, 2010).
- 61. Mirjalili, S. S. C. A. A sine cosine algorithm for solving optimization problems. Knowl. Based Syst. 96, 120-133 (2016).
- 62. Mohanty, B., Acharyulu, B. V. S. & Hota, P. K. Moth-flame optimization algorithm optimized dual-mode controller for multiarea hybrid sources AGC system. Optim. Control Appl. Methods 39, 720-734 (2017).
- 63. Mirjalili, S. S. C. A. A sine cosine algorithm for solving optimization problems. Knowl. Based Syst. 96, 120-133 (2016).
- 64. Kazarlis, S. A., Bakirtzis, A. G. & Petridis, V. A genetic algorithm solution to the unit commitment problem. IEEE Trans. Power Syst. 11, 83-92 (1996).
- 65. Jabari, M. et al. A novel artificial intelligence based multistage controller for load frequency control in power systems. Sci. Rep. 14, 66 (2024).
- Taher, A. S. & Reza, H. Robust decentralized load frequency control using multi variable QFT method in deregulated power systems. Am. J. Appl. Sci. 5, 818-828 (2008).
- 67. Erlich, I., Venayagamoorthy, G. K. & Worawat, N. A mean-variance optimization algorithm. IEEE Cong. Evol. Comput. 1, 1-6 (2010).
- Cheng, M. Y. & Prayogo, D. Symbiotic organisms search: A new metaheuristic optimization algorithm. Comput. Struct. 139, 98-112 (2014).
- 69. Khodabakhshian, A. & Hooshmand, R. A new PID controller design for automatic generation control of hydropower system. Electr. Power Energy Syst. 32, 375-382 (2010).
- 70. Du, D., Simon, D. & Ergezer, M. Biogeography-based optimization combined with evolutionary strategy and immigration refusal. In Proceedings of the IEEE Proceedings of the International Conference on Systems, Man and Cybernetics, San Antonio, TX, USA vol.
- 71. Rashedi, E., Nezamabadi-Pour, H. & Saryazdi, S. B. G. S. A. Binary gravitational search algorithm. Nat. Comput. 9, 727-745 (2010).
- 72. Sahu, P. C., Prusty, R. C. & Panda, S. Approaching hybridized GWO-SCA based type-II fuzzy controller in AGC of diverse energy source multi area power system. J. King Saud Univ. Eng. Sci. 32, 186-197 (2020).
- 73. Sahu, P. C., Mishra, S., Prusty, R. C. & Panda, S. Improved-salp swarm optimized type-II fuzzy controller in load frequency control of multi area islanded AC microgrid. Sustain. Energy Grids Netw. 16, 380-392 (2018).
- 74. Yang, X. S. Flower pollination algorithm for global optimization. Unconv. Comput. Nat. Comput. 1, 2409-2413 (2012).
- 75. Arora, K. et al. Optimization methodologies and testing on standard benchmark functions of load frequency control for interconnected multi area power system in smart grids. Mathematics 8, 980. https://doi.org/10.3390/math8060980 (2020)
- 76. Sahu, P. C., Prusty, R. C. & Panda, S. Improved-GWO designed FO based type-II fuzzy controller for frequency awareness of an AC microgrid under plug in electric vehicle. J. Ambient Intell. Hum. Comput. 12, 1879-1896 (2020).
- 77. Mishra, D., Sahu, P. C., Prusty, R. C. & Panda, S. Power generation monitoring of a hybrid power system with I-GWO designed trapezoidal type-II fuzzy controller. Int. J. Model. Simul. 42, 797-813 (2021).
- Hashim, Z. S. et al. Robust liquid level control of quadruple tank system: A nonlinear model-free approach. Actuators 12, 119. https://doi.org/10.3390/act12030119 (2023).

#### Acknowledgements

The authors extend their appreciation to Taif University, Saudi Arabia, for supporting this work through the Project Number TU-DSPP-2024-14. The authors express their sincere gratitude to the LEPCI Laboratory of the University of Ferhat Abbas Sétif-1, Algeria, for providing particular assistance in preparing this article.

#### **Author contributions**

Faycal Medjili, Abderrahmen Bouguerra, Mohamed Ladjal, and Badreddine Babes: Conceptualization. Methodology. Software. Visualization. Investigation. Writing—Original draft preparation. Enas Ali, Dessalegn Bitew Aeggegn, Ahmed B. Abou Sharaf: Data curation. Validation. Supervision. Resources. Writing—Review & Editing. Sherif S. M. Ghoneim: Project administration. Supervision. Resources. Writing—Review & Editing.

#### **Funding**

This research was funded by Taif University, Taif, Saudi Arabia (Project No. TU-DSPP-2024-14).

#### **Declarations**

#### Competing interests

The authors declare no competing interests.

#### Additional information

Correspondence and requests for materials should be addressed to D.B.A.

Reprints and permissions information is available at www.nature.com/reprints.

**Publisher's note** Springer Nature remains neutral with regard to jurisdictional claims in published maps and institutional affiliations.

**Open Access** This article is licensed under a Creative Commons Attribution-NonCommercial-NoDerivatives 4.0 International License, which permits any non-commercial use, sharing, distribution and reproduction in any medium or format, as long as you give appropriate credit to the original author(s) and the source, provide a link to the Creative Commons licence, and indicate if you modified the licensed material. You do not have permission under this licence to share adapted material derived from this article or parts of it. The images or other third party material in this article are included in the article's Creative Commons licence, unless indicated otherwise in a credit line to the material. If material is not included in the article's Creative Commons licence and your intended use is not permitted by statutory regulation or exceeds the permitted use, you will need to obtain permission directly from the copyright holder. To view a copy of this licence, visit <a href="https://creativecommons.org/licenses/by-nc-nd/4.0/">https://creativecommons.org/licenses/by-nc-nd/4.0/</a>.

© The Author(s) 2025